Addressing Barriers to Efficient Renewable Integration

Milestone Report 3

Lead Organisation: University of New South Wales (UNSW)

Project Partners: AEMO, ElectraNet, TasNetworks

Project Commencement Date: 02 July 2018

Project Completion Date: 02 July 2021

Authors: Leonardo Callegaro, Awais Ahmad, Georgios Konstantinou, Jenny Riesz, John Fletcher, Iain MacGill

Contact Name: John Fletcher

Title: Professor, School of Electrical Engineering and Telecommunication

Email: john.fletcher@unsw.edu.au

Date: 08 February 2020

Project Information: https://arena.gov.au/projects/addressing-barriers-efficient-renewable-integration/

Inverter Bench Testing Results: http://pvinverters.ee.unsw.edu.au

This activity received funding from *Australian Renewable Energy Agency* (*ARENA)* as part of *ARENA's Emerging Renewables Programme*. The views expressed herein are not necessarily the views of the Australian Government, and the Australian Government does not accept responsibility for any information or advice contained herein.

EXECUTIVE SUMMARY

Reliable and economic integration of distributed energy resources (DERs), such as rooftop photovoltaics (PV) with energy storage, introduces specific challenges resulting from their widespread growth. The integration of DERs impacts both the steady-state and the dynamic behaviour of the Bulk Power System (BPS). The safe operation of the BPS depends upon improvements in forecasting, monitoring, modelling and interconnection requirements. These improvements will facilitate the operation and enhance the reliability of the BPS with increased penetration of DER. The penetration of DERs in the Australian National Electricity Market (NEM) has increased significantly in the past decade. It is therefore crucial to develop accurate DER models for BPS studies in the NEM. To partially address this task, the Australian Renewable Energy Agency (ARENA) under the Emerging Renewable Program has funded this project to develop accurate models to represent the aggregate behaviour of various DERs and loads operating in Australia. The aim of this project is to develop a generic aggregate DER and composite load model (PV-Load model) that can be used for real-time and look-ahead studies in BPSs.

This technical report presents the details and findings for the project "Addressing barriers to efficient integration of renewables", for the period 15 Jul 2019 to 08 Feb 2020. The specific topics discussed in this report include:

Task 1 Providing options for managing high levels of rooftop PV, given findings and ongoing progress of the load monitoring program.

Task 2 Providing results of modelling from Milestone 2.

A summary of the progress accomplished on each deliverable is reported below.

Task 1.1 Bench testing of PV inverters. Laboratory tests on additional PV inverters have confirmed issues previously identified in Milestone 1 and 2. In detail, inverters can suddenly cease to deliver power, or disconnect from the grid due to the action of certain type of disturbances, identified as phase-angle jumps, short duration voltage sags and rate of change of frequency. These behaviours are a threat for the stability of power systems with high PV penetration, as large amounts of PV generation can suddenly be removed due to grid disturbances.

Task 1.2 Engagement with Standards Australia - The results from bench testing were communicated to the EL-42, the working group driving the revision of AS4777.2:2015. This standard addresses specification, functionality and testing of inverters connecting to the grid at low-voltage. The updated version of the standard, to be released in 2020, will require that inverters withstand phase angle jump tests, low voltage ride-through and rate of change of frequency.

Task 3 Load modelling progress - A computational tool to estimate and tune the composite PV-load model parameters has been devised. The tool uses measurements from grid disturbances to tune model parameters for the WECC model, previously implemented in Siemens PSSE software, under milestone 1 and milestone 2. This model is currently used by AEMO to forecast load, generation and for contingencies planning. The tool uses nonlinear programming techniques and estimates the model parameters by minimizing the deviation between computed and measured active and reactive power during a grid disturbance event. The model parameters estimated by this tool are different from the parameters of the WECC model and are a better fit for the load present in the Australian grid. With respect to milestone 2, which only included a load model without the DER_A component, the load model developed for milestone 3 includes the loads and well as the DER_A component representing the aggregate rooftop PV.

Contents

List of Figures

List of Tables

1 BENCH TESTING OF PV INVERTERS

Power electronic inverters are the key technology interfacing rooftop solar modules to the ac grid. As of July 2019, rooftop PV systems with power less or equal than 10 kW add up to 6.8 GW in Australia [13]. Each individual PV system of power less than 10 kW is uniquely controlled by the firmware programmed in the PV inverter, which complies with the specifications given in AS 4777.2:2015 [4]. Notwithstanding the functionality requirements mandated by [4], PV inverters appear to be vulnerable toward grid disturbances, which can cause bulk disconnections of distributed PV generation, with detrimental effects on power system stability and security [14, 15]. To understand the reasons behind large amount of distributed PV disconnections resulting from various grid events [14], a subset of the most popular rooftop PV inverters installed in Australia have been selected and tested for a set of grid disturbances, which are outside the scope of [4].

in the test setup, each inverter is connected to a PV emulator and a grid emulator via an interfacing inductance L_{g}, representing the grid impedance, as portrayed in Fig. 1.

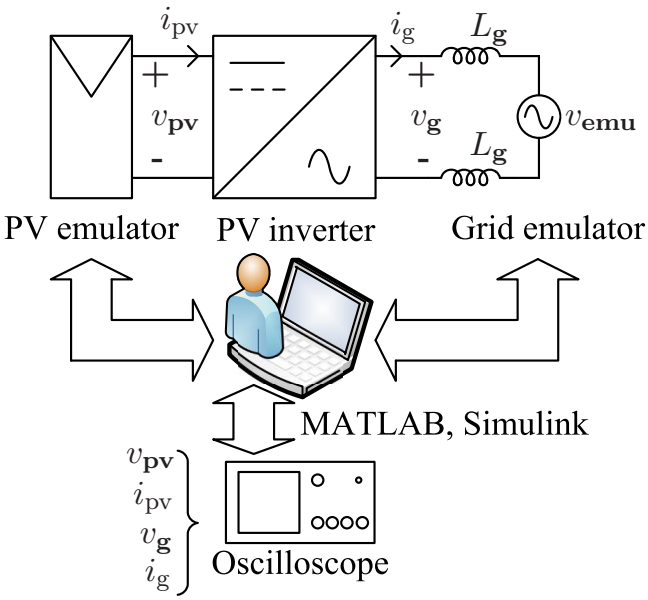

Figure 1: Schematic of the experimental setup

The behaviour of each inverter is verified when the parameters of the grid voltage (v_{g}) at the point of connection of the inverter are changed, by means of variations in the grid emulator voltage (v_{emu}) parameters. These are voltage phase-angle, frequency and voltage magnitude.

The work completed so far under Milestones 1 and 2 identified grid disturbance causing

Table 1: Cumulative power in GW of PV systems with size up to 10 kW installed to date in Australia [13]

	NSW	VIC	QLD	SA	WA	TAS	NT	NEM
GW	1.5	1.29	2.1	0.79	0.94	0.11	0.05	6.78

Table 2: Power from the inverter tested so far, obtained by multiplying the number of units installed by the power rating of each unit

	NSW	VIC	QLD	SA	WA	TAS	NT	NEM
MW	253	227	516	149	112	21	10	1288

several inverters to display an undesired behaviour, resulting in disconnection and output power curtailment leading to loss of distributed PV generation for several minutes, or reduction of output power for a few seconds. These disturbances are:

- Short duration voltage sag: from 230 V to 50 V for 100 ms
- Phase-angle jump: 15°, 30°, 45°, 90°
- Rate of change of frequency: 1 Hz/s, 4 Hz/s, 10 Hz/s

The scope of this report is to provide updated figures on the number of inverters which were tested against these disturbances and which have reported an undesired behaviour as a response.

As of July 2019 the distribution of rooftop systems with power up to 10 kW in each state of the National Electricity Market (NEM) is reported in Table 1

The number of inverters tested multiplied by the rated power of each inverter yields to the figures in Table 2, displaying the distributed power in each state and in the NEM from rooftop PV inverter models subjected to bench testing. The data in Table 2 have been obtained by multiplying the rated power of each inverter by the number of units of each inverter installed in the field; the latter data being gathered from the Clean Energy Regulator database. Overall, 19% (1.28 GW/6.78 GW) of all inverters in the NEM have been tested. So far, a total of 25 inverters from 11 different manufacturers have been tested.

Short-duration voltage sag An overview of the test results for the 230 V - 50 V, 100 ms voltage sag are given on Table 3. The actual power from inverters tested which are reflected in the NEM and which do not ride-through the short-duration voltage sag test is reported in Table 4.

Table 3: Summary of inverter behaviors due to short duration voltage sag

	2005 inverters			2015 inverters		
	Inv.	**Brand**	**Total**	**Inv.**	**Brand**	**Total**
Nºof inv. riding through	1/14	A/E	2	1,6,7/3,13,19/5/17 22/23	A/C/E/G J/K	9
Nºof inv. disconnecting	8/15/18,21	A/F/I	4	11/20	F/H	2
Nºof inv. curtailing ($P > 0$)	-	-	-	2/16	B/D	2
Nºof inv. curtailing ($P = 0$)	-	-	-	4, 10, 12	D	3
Nºof inv. with other behavior	6,24/9	A/B	3	-	-	-
Total Nºof inv. tested			9			16

Table 4: Cumulative power of inverters tested not riding-through the short duration voltage sag test. The percentage figure is obtained by dividing the power reported in the table by the total DER power in a state or the NEM (considering DER of power up to 10 kW)

	NSW	**VIC**	**QLD**	**SA**	**WA**	**TAS**	**NT**	**NEM**
MW - prev. Milestone	24	37	43	16	15	2	1	138
%	2	3	2	2.0	2	2	2	2
MW - this Milestone	105	91	116	46	32	6	3	398
%	7	7	6	6	3	6	5	6

Table 5: Power loss due to disconnection or curtailment caused by fast voltage sag, under the hypothesis that all inverters in the NEM behaves like the inverters tested so far

	NSW	**VIC**	**QLD**	**SA**	**WA**	**TAS**	**NT**	**NEM**
MW - prev. Milestone	361	527	292	278	303	29	9	1549
%	24	41	14	35	32	26	16	23
MW - this Milestone	620	513	472	244	268	33	13	2095
%	41	40	23	31	29	30	25	31

The absolute figures in Table 4 were obtained by multiplying the rated power of the inverter makes and models which do not ride through the short-duration voltage sag according to the test results, times the actual number of these inverters installed in the field. The percentage values in Table 4 have been calculated dividing the absolute power figure in the same table by the total power given by PV installations with power up to 10 kW present in each state and in the NEM, and summarised in Table 1. For instance, the number regarding this milestone report for NSW show that 105 MW of power is vulnerable to short-duration voltage sag disturbance. When this number is divided by 1.5 GW of PV generation installed in NSW (Table 1), then it results that 7% of installed PV generation is vulnerable to the short-duration voltage sag disturbance.

The inverters tested so far amount to 19% of the total installed rooftop PV capacity in the NEM, obtained by dividing the 1.28 GW figure in Table 2 by the 6.78 GW figure in Table 1 and 25 inverters from 11 different manufacturers have been tested.

Under the simplifying *assumption* that the distribution of inverter makes and models in the NEM is identical to the distribution of the inverters we have tested, in other words as if the whole rooftop PV power of systems under 10 kW is composed of the same 25 inverters tested so far, then figures on the DER power which is vulnerable to short-duration voltage sags can be extrapolated for NEM. The procedure to obtain the data reported in Table 5 is the following, with an example made for the NSW column:

- the cumulative power of inverters tested is obtained from Table 2 (e.g. 250 MW for NSW)
- the *actual* power which is vulnerable to short-duration voltage sag is obtained from Table 4 (e.g. 105 MW for NSW)
- under the simplifying *assumption* stated above, the power which is vulnerable to the short-duration voltage sag disturbance is extrapolated with the following method:
  - the *actual* power from inverters vulnerable to short-duration voltage sag (Table 4) is divided by power from inverters tested in Table 2 (e.g. 105 MW/253 MW = 0.415 for NSW, i.e. 42%)
  - the *extrapolated* absolute power from inverters failing the short-duration voltage sag test is calculated by multiplying the number previously calculated by the total power installed in a state or in the NEM, reported in Table 1 (e.g. 0.415×1.5 GW $\approx$ 620 MW for NSW, reported in Table 5)
  - the *extrapolated* percentage power from inverters failing the short-duration voltage sag test, is derived by dividing the absolute power value calculated above by the absolute value of DER power installed in a state or in the NEM reported in Table 1 (e.g. 620 MW/1.5 GW $\approx$ 41% for NSW, reported in Table 5)

In conclusion, the additional inverters which were tested under Milestone 3 have also shown to be vulnerable to the short-duration voltage sag disturbance. Considering all inverters tested thus far, and assuming that the distribution of inverters installed in the NEM is the same as the one of inverters tested, then vulnerability to short-duration voltage sag is estimated to affect about 31% of DER power from rooftop PV systems, that is 2.095 GW out of 6.78 GW.

Inverter Response to Phase-Angle Jump Disturbance Previous Milestone Reports 1 and 2 have documented the detrimental effect of phase-angle jumps on the correct operation of PV inverters, with certain inverters curtailing power or disconnecting from the ac grid due to this type of disturbance. This paragraph provides an update on the inverters which were lab-tested and which have displayed undesired behaviours upon the application of a phase-angle jump disturbance in the grid voltage.

Table 6 and Table 7 display the phase-angle jump test results for each inverter, where the check-mark "✓" indicates that the inverter rides through the phase-angle jump without any significant change of output power, the cross "X" indicates the disconnection of the inverter from the ac grid following the phase angle jump. The sign "P=0" indicates a power reduction to zero, while "curtail" means that the power output was reduced, but remained greater than zero; in such cases the inverter would require more than 5 min to resume operation at the pre-fault power level.

Table 6: Phase-angle-jump tests for 2005 inverters

Inv.	**Brand**	**15°**	**30°**	**45°**	**90 °**
1	A	✓	✓	✓	✓
6	A	✓	✓	✓	✓
8	A	✓	✓	✓	X
9	B	✓	✓	X	X
14	E	✓	✓	✓	X
15	G	✓	X	X	X
18	I	✓	✓	✓	✓

Table 7: Phase-angle-jump tests for 2015 inverters

Inv.	Brand	15°	30°	45°	90°
1	A	✓	X	-	-
2	B	✓	curtail	X	X
3, 13	C	✓	✓	✓	✓
4	D	P=0	curtail	P=0	P=0
5	E	✓	✓	✓	✓
6	A	✓	X	X	X
7	A	✓	curtail	P=0	P=0
10	D	P=0	P=0	P=0	P=0
11	F	X	X	-	-
12	D	P=0	P=0	P=0	P=0
13	C	✓	✓	✓	✓
16	D	✓	✓	✓	curtail
17	G	✓	✓	✓	✓
19	A	✓	✓	curtail	P=0
20	H	✓	✓	X	X
21	I	✓	✓	✓	✓
22	J	✓	✓	✓	✓
23	K	✓	curtail	curtail	curtail
24	A	✓	✓	✓	✓

Table 8 presents a summary of inverters which did not ride-through the phase-angle jump test, for a phase angle jump of 15°, 30°, 45° and 90°. The absolute power value in this table were obtained by multiplying the power rating of the inverters tested not riding-through each phase-angle jump test by the number of units installed in the field. The percentage values were obtained by dividing the absolute power values in Table 8 by the figures given in Table 1.

Table 8: Cumulative power of inverters not riding-through phase-angle-jump tests (note: the percentage figure is a ratio between the cumulative power in MW and the total DER power of inverters up to 10 kW installed in a state or in the NEM)

Not riding through PAJ		**NSW**	**VIC**	**QLD**	**SA**	**WA**	**TAS**	**NT**	**NEM**
15°	MW - prev. Miles	5	13	11	3	4	1 5	0	36
	%	0.3	1.0	0.5	0.4	0.4	0.9	0	0.5
15°	MW - this Miles	7	13	12	5	5	1	0	42
	%	0.4	1.0	0.6	0.6	0.5	0.9	0	0.6
30°	MW - prev. Miles	20	32	34	11	11	2	1	113
	%	1	3	2	1	1	2	2	2
30°	MW - this Miles	40	59	39	14	37	2	1	192
	%	2.7	4.6	1.9	1.7	3.9	1.8	1.6	2.8
45°	MW - prev. Miles	34	39	54	22	17	3	4	173
	%	2	3	3	3	2	2	8	3
45°	MW - this Miles	97	99	116	44	55	6	6	423
	%	7	8	6	6	6	5	11	6
90°	MW - prev. Miles	43	50	145	28	23	6	5	299
	%	3	4	7	4	2	6	9	4
90°	MW - this Miles	114	117	259	54	62	10	6	623
	%	8	9	12	7	7	9	12	9

As discussed for the short-duration voltage sag test, if the distribution of inverters installed in the NEM was identical to the distribution of inverters tested in the lab, an extrapolated projection on the power disconnecting or curtailing in each state is possible, and is reported in Table 9.

Table 9: Extrapolated power vulnerable to phase-angle jump disturbances, under the assumption that the distribution of inverters in the NEM is identical to the distribution of inverters bench-tested

Not riding through PAJ		NSW	VIC	QLD	SA	WA	TAS	NT	NEM
15°	MW - prev. Miles	71	188	73	54	78	12	0	410
	%	5	15	3	7	8	11	0	6
15°	MW - this Miles	40	76	47	24	42	5	0	222
	%	3	6	2	3	4	4	0	3
30°	MW - prev. Miles	307	462	235	195	236	22	8	1266
	%	20	36	11	25	25	20	15	19
30°	MW - this Miles	239	335	159	72	310	10	5	1010
	%	20	36	11	25	25	20	15	19
45°	MW - pre. Miles	515	558	368	371	360	30	42	1947
	%	34	43	18	47	38	27	78	29
45°	MW - this Miles.	577	561	470	233	463	30	31	2224
	%	39	44	22	29	49	27	58	33
90°	MW - prev. Miles	639	722	990	483	470	73	43	3366
	%	43	56	47	61	50	65	80	50
90°	MW - this Miles	673	663	1054	287	523	54	33	3276
	%	45	52	50	36	56	49	61	48

Table 10: Summary of inverter behaviors caused by RoCoF stimuli

	2005 inverters			2015 inverters		
	Inv.	Brand	Total	Inv.	Brand	Total
Nºof inv. disconnecting @ 10 Hz/s	-	-	-	4	D	1
Nºof inv. disconnecting @ 1, 4, 10 Hz/s	14	E	1	5	E	1
Nºof inv. riding through @ 1, 4, 10 Hz/s	all others		8	all others		14
Total Nºof inv. tested			5			16

Bench testing results obtained by applying phase-angle jump disturbances demonstrated very different outcomes depending on the inverter make and models. Cases where the inverter is disconnected from the ac grid following a phase-angle jump, or the inverter output power is curtailed to zero, albeit without a physical disconnection from the grid, are of particular concern. Almost 20% af all power from DER installed in the NEM is vulnerable to 30° phase-angle jump, according to the extrapolated figures reported in Table 9, and this percentage increases for more severe phase-angle jump values.

This paragraph gives a update on issues caused to PV inverters by rate of change of frequency in the grid voltage. The PV inverters tested under the Milestone 3 period have not demonstrated issues with respect to RoCoF in the grid voltage.

Table 11: Cumulative power of inverters not riding-through RoCoF. The percentage figure is a ratio between the power reported in the table and the total DER power in a state or the NEM, for DER up to 10 kW

Not riding through 1 Hz/s RoCoF		**NSW**	**VIC**	**QLD**	**SA**	**WA**	**TAS**	**NT**	**NEM**
Inv. 5 & Inv. 14	MW - prev. Miles %	22 1	21 2	165 8	12 2	9 1	5 5	0 1	234 3

Table 12: Power loss due to disconnection caused by RoCoF, under the hypothesis that all inverters in the NEM behaves like the inverters tested so far

Not riding through 1 Hz/s RoCoF		**NSW**	**VIC**	**QLD**	**SA**	**WA**	**TAS**	**NT**	**NEM**
Inv. 5 & Inv. 14	MW - prev. Miles %	323 22	301 23	1129 54	207 26	178 19	61 55	4 7	2629 39
Inv. 5 & Inv. 14	MW - this Miles %	128 9	119 9	672 32	64 8	72 8	27 24	2 4	1232 18

Table 10 reports a summary of inverter tested, including inverters disconnecting due to RoCoF in the grid voltage. None of the new inverters tested disconnected due to RoCoF. Therefore, the actual power which is vulnerable to RoCoF in the NEM is identical to the previous milestone and is reported in Table 11. Assuming that the distribution of inverters in the NEM is identical to the distribution of inverter tested, then an extrapolation of the power and percentage of inverter disconnecting due to RoCoF is reported in Table 12. Considering the extrapolated data gathered for this milestone, 18% of all inverters in the NEM are vulnerable to a RoCoF of 1 Hz/s. This figure has dropped from 39% presented in the previous milestone report, since more more inverters have now been tested, but the number of inverters whose operation is vulnerable to RoCoF has not increased compared to the previous milestone report.

1.1 Inverters Tested and Power Percentage in the NEM

Finally, based on the power rating of each inverter tested multiplied by the number of units installed, and based on the DER power of systems up to 10 kW (reported in Table 1), the percentage of inverters tested in each state and in the NEM is given Table 13. Overall, the inverters tested so far, represent 19% of the total power installed in the NEM (from PV systems of size up to 10 kW).

Table 13: Power percentage of each tested PV inverter in the National Energy Market

Inv.	Brand	Power (kW)	NSW	VIC	QLD	SA	WA	TAS	NT	NEM
1*	A	4.6	0.89%	0.45%	0.82%	1.27%	0.56%	0.60%	6.69%	0.83%
1**	A	4.6	1.08%	1.94%	3.50%	4.83%	0.92%	3.44%	3.79%	2.47%
2	B	4.6	0.79%	1.39%	1.01%	0.84%	0.66%	0.56%	1.57%	0.96%
3	C	4.99	1.84%	1.68%	3.11%	0.72%	1.57%	0.61%	1.29%	2.01%
4	D	4.6	0.00%	0.00%	0.00%	0.00%	0.00%	0.00%	0.00%	0.00%
5	E	5	0.90%	0.77%	3.54%	0.71%	0.37%	1.39%	0.56%	1.60%
6*	A	3	0.16%	0.06%	0.09%	0.13%	0.14%	0.08%	0.03%	0.11%
6**	A	3	0.43%	0.33%	0.35%	0.73%	0.38%	0.68%	0.15%	0.42%
7	A	4	0.10%	0.03%	0.03%	0.07%	0.02%	0.10%	0.04%	0.05%
8	A	5	0.02%	0.02%	0.05%	0.04%	0.03%	0.02%	0.02%	0.04%
9	B	3	0.03%	0.07%	0.10%	0.03%	0.07%	0.01%	0.00%	0.07%
10	F	4.6	0.00%	0.00%	0.00%	0.00%	0.00%	0.00%	0.00%	0.00%
11	D	4.2	0.01%	0.03%	0.01%	0.02%	0.01%	0.02%	0.00%	0.01%
12	D	5	0.30%	1.00%	0.50%	0.38%	0.39%	0.92%	0.00%	0.52%
13	C	4.99	0.52%	0.22%	0.51%	0.04%	0.06%	0.07%	0.14%	0.33%
14	E	5	0.54%	0.86%	4.32%	0.81%	0.55%	3.23%	0.24%	1.85%
15	G	1.5	0.00%	0.00%	0.00%	0.00%	0.00%	0.00%	0.00%	0.00%
16	D	3	0.03%	0.07%	0.03%	0.04%	0.05%	0.03%	0.00%	0.04%
17	H	4.6	0.48%	0.19%	0.64%	0.21%	0.05%	0.67%	0.03%	0.38%
18	I	1.5	0.81%	0.27%	0.31%	0.38%	0.30%	0.02%	0.01%	0.41%
19	A	5	0.99%	0.40%	0.86%	0.85%	0.46%	0.93%	2.98%	0.76%
20	H	4.6	1.89%	2.17%	1.86%	1.68%	0.84%	1.80%	0.03%	1.75%
21	I	2	1.54%	1.27%	0.41%	0.63%	0.07%	0.78%	0.01%	0.81%
22	J	5	1.66%	1.41%	1.17%	1.52%	1.02%	1.89%	0.35%	1.35%
23	K	5	1.20%	2.07%	0.18%	0.09%	2.59%	0.16%	0.00%	1.09%
24	A	4	0.52%	0.91%	1.12%	2.63%	0.65%	1.20%	1.46%	1.06%
TOT.	A-K	N/A	16.88%	17.65%	24.61%	18.83%	11.90%	19.14%	19.39%	**19.01%**

*: Inverter 6 post 2015.
**: Inverter 6 pre 2015.

1.2 Conclusions

Bench-testing of PV inverters demonstrated that although inverters are compliant to AS 4777 standards, their operation is vulnerable to grid disturbances such as short-duration voltage sag, grid voltage phase-angle jump and rate of change of frequency. While previous milestone reports 1 and 2 described the experimental occurrence of undesired behaviours, such as inverter disconnection and power curtailment, this milestone report provides an update on the number of inverters which have been tested and have shown vulnerability towards grid disturbances.

Installed capacity from DER up to 10 kW is estimated to be 6.78 GW for the whole NEM [13]. The cumulative power from DER at risk of disconnection or curtailment in each state and in the NEM was estimated. Particularly significant were the extrapolated power estimates, showing the amount of DER power vulnerable to grid disturbances under the assumption that the distribution of inverters installed in the NEM is identical to the distribution of inverters tested in the lab. In such condition, the short-duration voltage sag disturbance my put at risk 31% of DER power in the NEM, the grid voltage phase-angle jump disturbance (for instance for a 30° phase-angle jump) may put at risk 19% of DER's in the NEM and a RoCoF of 1 Hz/s could be threatening 18% of all DER in the NEM.

2 ENGAGEMENT WITH STANDARDS AUSTRALIA

As a result of the engagement with the steering committee and industry advisory group members, which gave the opportunity to share the result of bench testing to several interested parties, Prof. John Fletcher and Dr Leonardo Callegaro are now embedded in the EL-04 committee of Standards Australia. This committee is currently updating the standard AS 4777.2 concerning the connection to th grid at low-voltage, and directly affecting PV inverters. The work to update this standard is divided among three major groups, dealing with *specifications*, *functionalities* and *testing*. Prof. Fletcher and Dr Callegaro are part of the *testing* group, and are involved in defining the tests and associated testing procedures to be part of the new standard. This activity will start after *specifications* and *functionalities* sub-groups complete their tasks in February/March 2020.

3 THE COMPOSITE LOAD MODEL

This section and Section 4 refer to work which was completed under Milestone 2. Readers interested to the load modelling update can skip to Section 5 of this report.

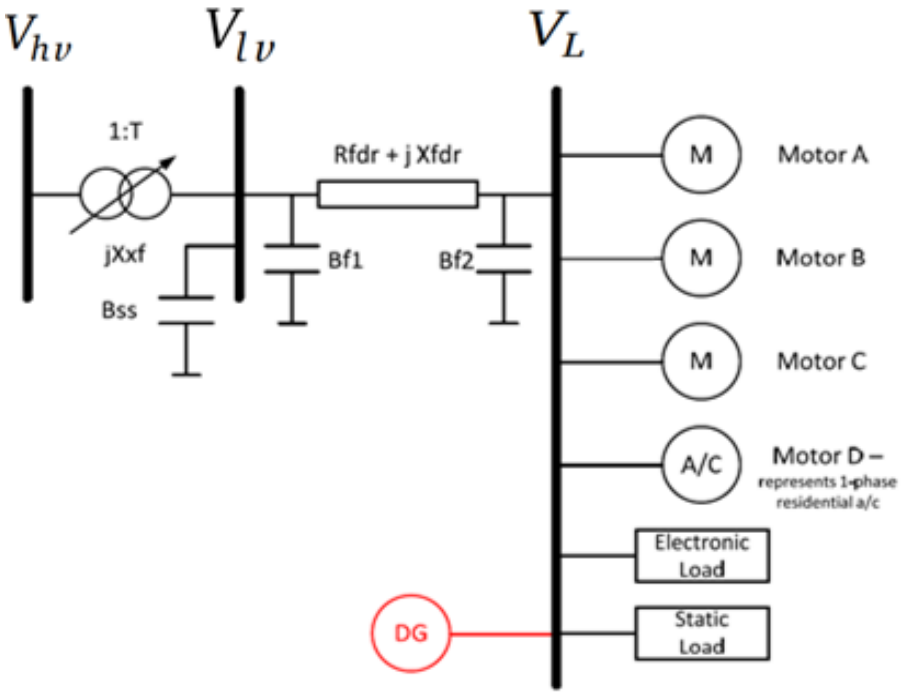

Figure 2: Diagram of the WECC Composite Load Model (WECC-CMLD).

3.1 WECC-CMLD Description

Exhaustive international work has paved the way towards the development of more precise composite load models for power system dynamic simulations. Recently, the Western Electricity Coordinating Council (WECC) proposed a generic composite load model that includes a representation of the distribution feeder, and the aggregate behaviour of various loads and DERs connected in distribution systems. A diagram of the WECC composite load model (WECC-CMLD) is depicted in Fig 2. Each component of the model can be described as follows:

- **Motor A:** Three-phase induction motor with low inertia which represents the aggregate behaviour of motors driving loads with constant torque, such as commercial and residential air conditioning and refrigerator compressors. This model should not be used to represent the dynamics of residential loads.

- **Motor B:** Three-phase induction motor with large inertia which represents the dynamics of commercial ventilation fan motors and air-handling systems.
- **Motor C:** Three-phase induction motors with low inertia driving loads whose torque is proportional to speed squared. Typically includes motors found in commercial water circulation pumps in central cooling systems
- **Motor D:** Single-phase induction motors representing primarily residential air conditioner compressor motors. In Australia, air conditioning loads might be connected to the grid via power electronic converters, this must be further investigated.
- **Power electronic loads:** Inverter-based or electronically coupled loads.
- **Static loads:** Other types of loads not explicitly modelled in the other components. Includes lighting, small electrical household and small commercial loads.

It is important to mention that the motors and the power-electronic-load components of the WECC-CMLD have an accurate model of their protection equipment (relay model for motors). This is to represent the behaviour of the devices when exposed to extreme disturbances in the power grid. When a disturbance exceeds the upper and lower limits of operation of each device, the protection equipment trips the appliance after an inherent delay. This action of the protective relay is reflected in the model by tripping the appliance from the WECC-CMLD.

One of the greatest challenges when developing the WECC-CMLD is the identification of the critical parameters of each component—specifically the load fractions and the undervoltage protection settings. One possible solution is to conduct surveys on the types of residential and commercial loads connected in various feeders of the distribution networks in Australia. Unfortunately, the parameters derived from past surveys have some degree of inaccuracy. This inherent error can be reduced by calibrating the parameters using measurement-based estimation. The measurement-based load modelling aims at deriving the load model parameters directly from disturbance measurements at different substations, times of the day, weather conditions and so on. In this section, the dynamic equations and parameters of the WECC-CMLD are described in detail. Next, in Section 4, the derived model will be used to estimate the most influential parameters using a measurement-based load modelling approach.

3.2 WECC-CMLD Equations and Parameters

This sections gives a thorough description of each load component of the WECC-CMLD. The DG component (DER_A) was explained in the Milestone 1 report.

3.2.1 Distribution Transformer and Feeder

The first component in the WECC-CMLD is the substation transformer (Xxf) along with an on-load tap-changer (OLTC) control, substation shunt-capacitors (B_{ss}) and the feeder interconnecting the sub-transmission network with the distribution system. As indicated in Fig. 2, the voltage at the primary-side (or high-voltage side) of the tap changer transformer is V_{hv} and the voltage at the secondary-side (or low-voltage side) is V_{lv}. The TAP of the substation transformer is determined by the following equation [10]:

$$TAP = \sqrt{\frac{V_{hv}((V_{min} - V_{max})/2)^2}{(Q_L X_{xfr} - V_{hv})^2 + (X_{xfr} P_L)}} \tag{1}$$

where P_L and Q_L are the active and reactive power entering at the load bus. The TAP of the transformer is constrained to minimum and maximum values of T_{min} and T_{max} respectively. Additionally, the adjustment of TAP positions and its control have an inherent delay represented by parameters TD and TC respectively. Using equation 1, the voltage at the secondary winding of the tap changer V_{lv} can be determined as follows [10]:

$$V_{lv} = TAP \frac{T_{fixls}}{T_{fixls}} (V_{hv} - jX_{xfr} T_{fixhs} I_{hs}), \tag{2}$$

where I_{hv} is the current at the primary-side of the transformer. Finally, the voltage at the load bus V_L can be calculated using V_{lv} and I_{hv}, as follows:

$$V_L = V_{lv} - (R_{fdr} + jX_{fdr})(I_{hv} T_{fixhs}/(TAP \cdot T_{fixls}) - jB_{ss} V_{lv}) \tag{3}$$

The default parameters related to each of these components are given below.

- Substation compensation B_{ss}; pu on load base: **0**
- Rfdr - Feeder resistance; pu on load base: **0.04**
- Xfdr - Feeder reactance; pu on load base: **0.04**
- Xxf - Transformer reactance; pu on load base: **0.08**

- Tfixhs - High side fixed transformer tap: **1**
- Tfixls - Low side fixed transformer tap: **1**
- LTC - LTC flag (1=active; 0=inactive): **1**
- Tmin - LTC min tap (on low side): **0.9**
- Tmax - LTC max tap (on low side): **1.1**
- Step - LTC Tstep (on low side): **0.0063**
- Vmin - Min value of V target range on xfr low side: **1**
- Vmax - Max value of V target range on xfr low side: **1.02**
- TD - LTC control time delay; s: **30**
- TC - LTC tap adjustment time delay; s: **5**

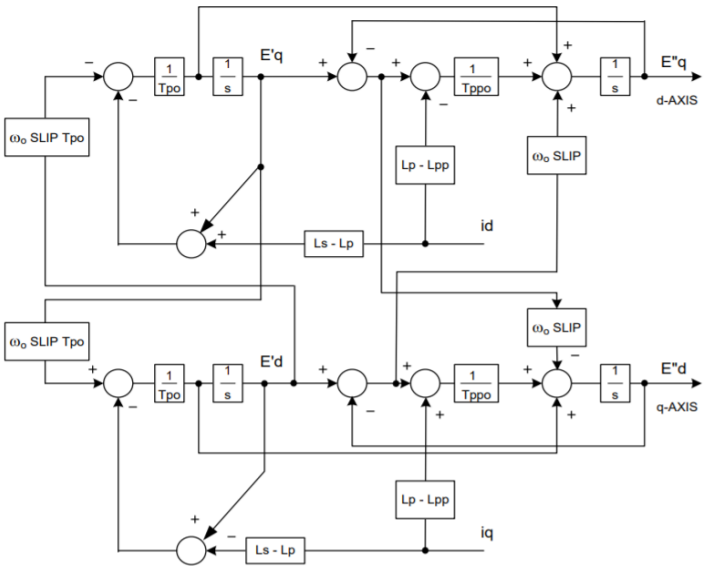

Figure 3: Block diagrams of Motor A,B and C in the WECC-CMLD [9].

3.2.2 Three-phase Induction Motors (Motor A, B and C)

Each induction motor $k \in \{A, B, C\}$ is represented by a set of nonlinear algebraic and differential equations. A block diagram for the model of motor k is depicted in Fig. 3. The fifth-order dynamical model for motor k is governed by vector of state variables $\mathbf{x}_k =$

$[E_q^{'}, E_q^{'}, E_q{''}, E_d{''}, \omega]^T$, a vector of parameters $\mathbf{z}_k = [T_0^{'}, T_0^{''}, L_s, r_s, L^{'}, L^{''}, H, E_{trq}, F_{mk}, LF]^T$, a vector of algebraic variables $\mathbf{c}_k = [i_d, i_q, Slip]^T$ and a vector of inputs $\mathbf{v}_k = [V_d, V_q]^T$. For the sake of clarity, we avoid adding the subscript k in the variables and parameters of each motor, however, we advise the reader that these variables are different for each induction motor. The parameters for three-phase induction motor k are explained below:

- F_{mk} - Motor A, B, C composite load motor fractions F_{mA}, F_{mB}, F_{mC}: **0.12**, **0.14**, **0.1**
- LF - Motor A, B, C real power to power base ratio: **0.75**, **0.75**, **0.75**
- r_s - Motor A, B, C stator resistance, pu on motor base: **0.04**, **0.03**, **0.03**
- $X_s(\omega L_s)$- Motor A, B, C synchronous reactance, pu: **1.8**, **1.8**, **1.8**
- $X^{'}(\omega L^{'})$ - Motor A, B, C transient reactance, pu: **0.12**, **0.19**, **0.19**
- $X^{"}(\omega L^{''})$ - Motor A, B, C subtransient reactance, pu: **0.104**, **0.14**, **0.14**
- $T_o^{'}$ - Motor A, B, C transient open circuit time constant, s: **0.095**, **0.2**, **0.2**
- $T_o^{"}$ - Motor A, B, C subtransient open cir time constant, s: **0.0021**, **0.0026**, **0.0026**
- H - Motor A, B, C inertia constant: **0.1**, **0.5**, **0.1**
- E_{trq} - Motor A, B, C exponential for variation of torque with speed: **0**, **2**, **2**

The dynamic equations of each induction motor can be derived from the block diagram in Fig. 3, as follows:

$$\frac{dE_q^{'}}{dt} = \frac{-1}{T_0^{'}} E_q^{'} - \frac{1}{T_0^{'}}(L_s - L^{'}) i_d - \omega_0 Slip E_d^{'}, \tag{4}$$

$$\frac{dE_d^{'}}{dt} = \frac{-1}{T_0^{'}} E_d^{'} + \frac{1}{T_0^{'}}(L_s - L^{'}) i_d + \omega_0 Slip E_q^{'}, \tag{5}$$

$$\frac{dE_q^{''}}{dt} = \frac{T_0^{'} - T_0^{''}}{T_0^{'} T_0^{''}} E_q^{'} - \frac{E_q^{''}}{T_0^{''}} - \frac{(L_s - L^{'})T_0^{''} + (L^{'} - L^{''})T_0^{'}}{T_0^{'} T_0^{''}} i_d - \omega_0 Slip E_d^{''}, \tag{6}$$

$$\frac{dE_d^{''}}{dt} = \frac{T_0^{'} - T_0^{''}}{T_0^{'} T_0^{''}} E_d^{'} - \frac{E_d^{''}}{T_0^{''}} + \frac{(L_s - L^{'})T_0^{''} + (L^{'} - L^{''})T_0^{'}}{T_0^{'} T_0^{''}} i_q + \omega_0 Slip E_q^{''}. \tag{7}$$

$$\frac{d\omega}{dt} = -\frac{T_e - Tm}{2H}. \tag{8}$$

Where the electrical and mechanical variables of vector $\mathbf{c}_k$ are given by the algebraic equations (9)-(12).

$$i_d = \frac{r_s}{r_s^2 + L''^2}(V_d + E_d'') + \frac{L''}{r_s^2 + L''^2}(V_q + E_q'') \tag{9}$$

$$i_q = \frac{r_s}{r_s^2 + L''^2}(V_q + E_q'') + \frac{L''}{r_s^2 + L''^2}(V_d + E_d'') \tag{10}$$

$$Slip = 1 - \omega \tag{11}$$

$$Tm = T_{m0}\omega^{Etrq} \tag{12}$$

Using the model in equations (4)-(12), the active and reactive power outputs of induction motor k as functions of $\mathbf{x}_k$, $\mathbf{z}_k$, $\mathbf{c}_k$ and $\mathbf{v}_k$ can be calculated by the following equations:

$$P_{IM,k}(\mathbf{x}_k, \mathbf{z}_k, \mathbf{c}_k, \mathbf{v}_k) = V_d i_d + V_q i_q \tag{13}$$

$$Q_{IM,k}(\mathbf{x}_k, \mathbf{z}_k, \mathbf{c}_k, \mathbf{v}_k) = V_d i_q - V_q i_d \tag{14}$$

If the input voltage in steady-state is $\mathbf{v}_k^0$ and the active and reactive power at the load bus are P_L and Q_L respectively (obtained from the power flow solution in steady state), induction motor k has a initial steady-state power output of:

$$P_{IM,k}(\mathbf{x}_k, \mathbf{z}_k, \mathbf{c}_k, \mathbf{v}_k^0) = F_{mk} P_L \tag{15}$$

$$Q_{IM,k}(\mathbf{x}_k, \mathbf{z}_k, \mathbf{c}_k, \mathbf{v}_k^0) = F_{mk} Q_L \tag{16}$$

Parameter F_{mk} is known as *load-fraction*; it represents the fraction of active and reactive power dragged by induction motor k in the WECC-CMLD. The load fraction F_{mk} is used to obtain the initial conditions of the state variables of each motor k. More specifically, the initial conditions are obtained by solving for i_d and i_q in equations (13) and (14) with the initial active and reactive power values in (15) and (16). Using the values derived for i_d and i_q, the initial conditions of all the state variables can be obtained by solving for the equilibrium point $\mathbf{x}_k^*$ of equations (4)-(8) with $d\mathbf{x}_k/dt = 0$.

Motor k has a detailed model of its built-in protection equipment. The protection model has two levels of voltage tripping which can emulate a partial tripping of the motor when the terminal voltage exceeds the defined limits. The parameters of the protection mechanism are given in a user-defined parameter vector $\mathbf{z}_{prt,k} = [V_{tr1}, T_{tr1}, F_{tr1}, V_{rc1}, T_{rc1}, V_{tr2}, T_{tr2}, F_{tr2}, V_{rc2}, T_{rc2}]^T$. Each parameter is described as follows:

- V_{tr1} - Motor A, B, C 1st undervoltage trip voltage, pu: **0.65**, **0.55**, **0.58**
- T_{tr1} - Motor A, B, C 1st undervoltage trip delay, s: **0.1**, **0.02**, **0.03**
- F_{tr1} - Motor A, B, C 1st undervoltage trip fraction: **0.2**, **0**, **0**
- V_{rc1} - Motor A, B, C 1st undervoltage reclose voltage, pu: **0.1**, **0.65**, **0.68**
- T_{rc2} - Motor A, B, C 1st undervoltage reclose delay, s: **99999**, **0.05**, **0.05**
- V_{tr2} - Motor A, B, C 2nd undervoltage trip voltage, pu: **0.5**, **0.5**, **0.53**
- T_{tr2} - Motor A, B, C 2nd undervoltage trip delay, s: **0.02**, **0.025**, **0.03**
- F_{tr2} - Motor A, B, C 2nd undervoltage trip fraction: **0.75**, **0**, **0**
- V_{rc2} - Motor A, B, C 2nd undervoltage reclose voltage, pu: **0.65**, **0.6**, **0.62**
- T_{rc2} - Motor A, B, C 2nd undervoltage reclose delay, s: **0.1**, **0.05**, **0.1**

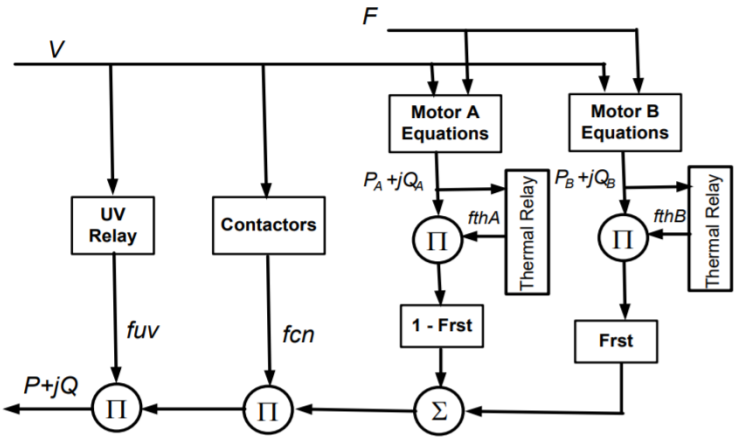

Figure 4: Block diagram of single-phase induction motor (Motor D) [9]

3.2.3 Single-Phase Induction Motor (Motor D)

This model is meant to represent the aggregate behaviour of single-phase air conditioners. A block diagram of the model for Motor D is depicted in Fig. 4. With this model, it is possible to determine the air conditioners active and reactive power and the power factor variation due to voltage and frequency disturbances. Another feature of the model is the possibility to emulate the motor stalling phenomenon. Both the motor current as well as the active and reactive power can be modelled in stalled state. Similar to the three-phase motors, partial tripping of motor D due to action of the protection equipment can be emulated by using appropriate under-voltage and thermal relay models. A brief description of each component shown in Fig. 4 will be provided below.

- **Compressor Motor Model**: This model represents the behaviour of compressor motors in both run and stall states. The model transitions from normal state to stall state if the terminal voltage is less than a user-defined stall voltage V_{stall} for an amount of time greater than T_{stall}. When the model operates in stall state, it is represented by an user-defined equivalent impedance $R_{stall} + jX_{stall}$. As shown in Fig. 4, the model is composed of two different motors, namely motor A and motor B, operating simultaneously in the simulation. Motor A represents the restartable compressor motors and B emulates the non-restartable ones. The model is mathematically respresented by a vector of inputs variables $\mathbf{v}_D = [V, \omega]^T$, a vector of parameters $\mathbf{z}_D = [K_{p1}, K_{p2}, K_{q1}, K_{q2}, V_{brk}, V_{stall}, N_{p1}, N_{p2}, N_{q1}, N_{q2}, CmpK_{pf}, CmpK_{qf}, CompPF, CompLF, T_{stall}, R_{stall},$
  In the run state, the characteristic equations between the active/reactive power and the voltage are exponential. The active power P_D and reactive power Q_D as functions of $\mathbf{v}_D$ and $\mathbf{z}_D$ in the run state are expressed are follows:

$$P_D(\mathbf{v}_D, \mathbf{z}_D) = \begin{cases} P_0 + K_{p1}(V - V_{brk})^{N_{p1}} & V_{brk} \leq V \\ P_0 + K_{p2}(V - V_{brk})^{N_{p2}} & V_{stall} \leq V \leq V_{brk} \end{cases} \tag{17}$$

$$Q_D(\mathbf{v}_D, \mathbf{z}_D) = \begin{cases} Q_0 + K_{q1}(V - V_{brk})^{N_{q1}} & V_{brk} \leq V \\ Q_0 + K_{q2}(V - V_{brk})^{N_{q2}} & V_{stall} \leq V \leq V_{brk} \end{cases} \tag{18}$$

  Where P_0 and Q_0 are obtained at $V = 1\ p.u$, as follows:

$$P_0 = F_{mD} P_L - K_{p1}(1 - V_{brk})^{N_{p1}}, \tag{19}$$

$$Q_0 = F_{mD}Q_L - K_{q1}(1 - V_{brk})^{N_{q1}}, \tag{20}$$

Where F_{mD} is the load fraction assigned to motor D. In order to emulate frequency dependency of the model, the active and reactive power in (17) and (18) are modified as follows:

$$P_D(\mathbf{v}_D, \mathbf{z}_D) \longleftarrow P_D(\mathbf{v}_D, \mathbf{z}_D)(1 + CmpK_{pf}\frac{\omega - \omega_0}{2\pi}) \tag{21}$$

$$Q_D(\mathbf{v}_D, \mathbf{z}_D) \longleftarrow Q_D(\mathbf{v}_D, \mathbf{z}_D)(1 + \frac{CmpK_{qf}(\omega - \omega_0)}{(1 - CompPF^2)2\pi}) \tag{22}$$

The parameters related to the compressor motor model as explained below:

- FmD - Composite load motor D fraction: **0.03**
- Tstall - Motor D stall delay time, s: **0.03**
- Trestart - Motor D restart from stall delay time, s: **0.3**
- CompLF - Motor D real power to motor base ratio: **1**
- CompPF - Motor D power factor at 1.0 pu voltage: **0.98**
- Vstall - Motor D stall Voltage, pu: **0.45**
- Rstall - Motor D stall resistance, pu of motor base: **0.1**
- Xstall - Motor D stall reactance, pu of motor base: **0.1**
- LFadj - Adjustment to stall voltage if COMPLF /= 1.0: **0**
- Kp1 - Motor D real power coeff when voltage $>$ Vbrk: **0**
- Np1 - Motor D real power exp when voltage $>$ Vbrk: **1**
- Kq1 - Motor D reactive power coeff when voltage $>$ Vbrk: **6**
- Nq1 - Motor D reactive power exp when voltage$>$Vbrk: **2**
- Kp2 - Motor D real power coeff when voltage $<$ Vbrk: **12**
- Np2 - Motor D real power exp when voltage $<$ Vbrk: **3.2**
- Kq2 - Motor D reactive power coeff when voltage $<$ Vbrk: **11**
- Nq2 - Motor D reactive power exp when voltage $<$ Vbrk: **2.5**
- Vbrk - Motor D ”break-down” voltage,: **0.86**
- Frst - Motor D fraction capable of restart after stall: **0.2**

- Vrst - Motor D voltage for restart after stall, pu: **0.95**
- CmpKpf - Motor D real power frequency dependency: **1**
- CmpKqf - Motor D reactive power freq dependency: **-3.3**

- **Contactor Model** Power contactor are used to energize the compressor motors. The status of the power contactor (1 or 0) depends entirely on the input voltage V. The input voltage V and frequency f are estimated using first-order lag filters with time constants T_v and T_f respectively. The parameters of the power contactor are given in vector $\mathbf{z}_{D,cnt} = [T_v, T_f, Vc1off, Vc2off, Vc1on, Vc2on]^T$. These parameters are explained below:
  - Tv - Motor D voltage time constant for contactors, s: **0.025**
  - Tf - Motor D frequency time constant for contactors, s: **0.1**
  - Vc1off - Motor D voltage contactors start opening, pu: **0.5**
  - Vc2off - Motor D voltage all contactors opened, pu: **0.4**
  - Vc1on - Motor D voltage contactors start closing, pu: **0.6**
  - Vc2on - Motor D voltage all contactors closed, pu: **0.52**
- **Under-voltage Relay Model**: If the terminal voltage exceeds the voltage thresholds for a specified amount of time, the motors are tripped from the simulation without reconnection. The under-voltage relay parameters are represented by vector $\mathbf{z}_{D,uv} = [F_{uvr}, UV_{tr1}, T_{tr1}, UV_{tr2}, T_{tr2}]^T$ and can be described as follows:
  - Fuvr - Motor D fraction with undervoltage relays: **0.1**
  - UVtr1 - Motor D 1st undervoltage pick-up, pu: **0.5**
  - Ttr1 - Motor D 1st undervoltage trip delay, s: **0.02**
  - UVtr2 - Motor D 2nd undervoltage pick-up, pu: **0.1**
  - Ttr2 - Motor D 2nd under voltage trip delay, s: **9999** s
- **Thermal Relay Model**: Air-conditioners are protected against over-heating using thermal relays. The winding temperature T_w can be calculated by equation (23), where i_c is the motor current, R_{stall} is the stall resistance and T_{th} is the motor heating time constant.

$$\frac{dT_w}{dt} = -\frac{1}{T_{th}}(i_c^2 * R_{stall} - T_w) \tag{23}$$

The thermal relay model emulates motor tripping by multiplying the active and reactive power of the motor by a fraction $0 \leq K \leq 1$. Using the computed winding temperature T_w, the model determines the value of K by comparing T_w with two user-defined parameters Th_{1t} and Th_{2t}. If $T_w < Th_{1t}$ then $K = 1$, otherwise, K is determined by linear interpolation between points $(1, Th_{1t})$ and $(0, Th_{2t})$. The thermal relay state variables parameters are represented by vectors $\mathbf{x}_{TR} = [T_w]$ and $\mathbf{z}_{D,tr} = [Th_{1t}, Th_{2t}]^T$ respectively.

The default values of the parameters of the thermal relay model are summarized as follows:

- Tth - Motor D heating time constant, s: **15**
- Th1t - Motor D temperature where tripping begins, pu: **0.7**
- Th2t - Motor D temperature where completely tripped: **1.9**

3.2.4 Electronic Loads

These loads are represented as constant active and reactive power when the terminal voltage V is greater than an user-defined voltage threshold V_{d1}. Both the active and reactive power are linearly decreased to zero if $V_{d2} \leq V \leq V_{d1}$. Voltage V_{d2} is a second user-defined voltage threshold that indicates the minimum voltage at which electronic loads remain connected. The input of the electronic loads is the vector $\mathbf{v}_{el} = [V]$ and parameters are placed in vector $\mathbf{z}_{el} = [V_{d1}, V_{d2}, F_{el}, PF_{el}]^T$, where F_{el} and PF_{el} are the load fraction and the power factor of the electronic loads respectively. That being said, the electronic loads consume an active and reactive of:

$$P_{el}(\mathbf{v}_{el}, \mathbf{z}_{el}) = \begin{cases} F_{el}\sqrt{P_L^2 + Q_L^2}PF_{el} & V_{d1} \leq V \\ F_{el}\frac{\sqrt{P_L^2+Q_L^2}PF_{el}}{V_{d1}-V_{d2}}(V - V_{d2}) & V_{d2} \leq V \leq V_{d1} \\ 0 & V \leq V_{d2} \end{cases} \tag{24}$$

$$Q_{el}(\mathbf{v}_{el}, \mathbf{z}_{el}) = \begin{cases} F_{el}\sqrt{P_L^2 + Q_L^2}\sin(\arccos(PF_{el})) & \\ F_{el}\frac{\sqrt{P_L^2+Q_L^2}\sin(\arccos(PF_{el}))}{V_{d1}-V_{d2}}(V - V_{d2}) & V_{d2} \leq V \leq V_{d1} \\ 0 & V \leq V_{d2} \end{cases} \tag{25}$$

The default values of the parameters of the electronic load model are summarized as follows:

– FeI - Composite load electronic fraction: **0.27**

– PFeI - Electronic load power factor: **1**

– Vd1 - Voltage electronic loads start to drop: **0.7**

– Vd2 - Voltage all electronic load has dropped: **0.5**

3.2.5 Static Loads

The active and reactive power of the static loads vary exponentially with respect to the input voltage V and linearly with respect to the load bus frequency f. The static load input vector is $\mathbf{v}_{st} = [V, \omega]^T$ and the parameter vector is $\mathbf{z}_{st} = [PFs, P_{1e}, P_{1c}, P_{2e}, P_{2c}, Q_{1e}, Q_{2e}, Q_{1c}, Q_{2c}, P_{frq}, Q_{frq}]^T$. The equations of active power (P_{ST}) and reactive power (Q_{ST}) of the static loads with respect to the inputs $\mathbf{v}_{st}$ and the parameters $\mathbf{z}_{st}$ are given by:

$$P_{ST}(\mathbf{v}_{st}, \mathbf{z}_{st}) = P_0(P_{1c}(\frac{V}{V_0})^{P_{1e}} + P_{2c}(\frac{V}{V_0})^{P_{2e}} + P_3)(1 + P_{frq}(\omega - \omega_0)/(2\pi)), \tag{26}$$

$$Q_{ST}(\mathbf{v}_{st}, \mathbf{z}_{st}) = Q_0(Q_{1c}(\frac{V}{V_0})^{Q_{1e}} + Q_{2c}(\frac{V}{V_0})^{Q_{2e}} + Q_3)(1 + Q_{frq}(\omega - \omega_0)/(2\pi)), \tag{27}$$

where P_0, Q_0, P_3 and Q_3 are given by:

$$P_0 = P_L(1 - F_{mA} - F_{mB} - F_{mC} - F_{mD} - F_{el}) \tag{28}$$

$$Q_0 = Q_L(1 - F_{mA} - F_{mB} - F_{mC} - F_{mD} - F_{el}) \tag{29}$$

$$P_3 = 1 - P_{1c} - P_{2c} \tag{30}$$

$$Q_3 = 1 - Q_{1c} - Q_{2c} \tag{31}$$

The parameters of the static loads and their default values are summarized as follows:

– PFs - Static load lower lactor: **1**

– P1e - First exponent for static load P: **1**

– P1c - First coeff for static load P: **0.48**

– P2e - Second exponent for static load P: **2**

- P2c - Second coeff for static load P: **0.52**
- Pfrq - Frequency sensitivity for static P: **0**
- Q1e - First exponent for static load Q: **1**
- Q1c - First coeff for static load Q: **0.48**
- Q2e - Second exponent for static load Q: **2**
- Q2c - Second coeff for static load Q: **0.52**
- Qfrq - Frequency sensitivity for static load Q: **-1**

3.3 Final WECC-CMLD States, Variables and Parameters

Based on the above discussion, the entire WECC-CMLD can be represented by a set of differential and algebraic equations. Let the state variable vector, parameter vector, algebraic variable vector and input vector of the entire WECC-CMLD be $\mathbf{x} = [\mathbf{x}_A^T, \mathbf{x}_B^T, \mathbf{x}_C^T, \mathbf{x}_{TR}^T]^T$, $\mathbf{z} = [\mathbf{z}_A^T, \mathbf{z}_{prt,A}^T, \mathbf{z}_B^T, \mathbf{z}_{prt,B}^T, \mathbf{z}_C^T, \mathbf{z}_{prt,C}^T, \mathbf{z}_D^T, \mathbf{z}_{D,cnt}^T, \mathbf{z}_{D,uv}^T, \mathbf{z}_{D,tr}^T, \mathbf{z}_{el}^T, \mathbf{z}_{st}^T]^T$, $\mathbf{c} = [\mathbf{c}_A^T, \mathbf{c}_B^T, \mathbf{c}_C^T]^T$ and $\mathbf{v} = [\mathbf{v}_A^T, \mathbf{v}_B^T, \mathbf{v}_C^T, v_D^T, \mathbf{v}_{el}^T, \mathbf{v}_{st}^T]^T$ respectively. The WECC-CMLD can be represented by the following equations:

$$\frac{d\mathbf{x}}{dt} = F(\mathbf{x}, \mathbf{z}, \mathbf{c}, \mathbf{v}), \tag{32}$$

$$0 = G(\mathbf{z}, \mathbf{c}, \mathbf{v}), \tag{33}$$

where function F contains equations (4)-(8) and equation (23) for all motors A, B, C and D. Function G is derived from equations (9)-(12) for all three induction motors. The outputs of the WECC-CMLD are the total active and reactive power consumed by all the components in the model, expressed as functions of time t, **x**, **z**, **c**, **v** in the following manner:

$$P_{cmld}(t, \mathbf{x}, \mathbf{z}, \mathbf{c}, \mathbf{v}) = P_{IM,A} + P_{IM,B} + P_{IM,C} + P_D + P_{el} + P_{ST} \tag{34}$$

$$Q_{cmld}(t, \mathbf{x}, \mathbf{z}, \mathbf{c}, \mathbf{v}) = Q_{IM,A} + Q_{IM,B} + Q_{IM,C} + Q_D + Q_{el} + Q_{ST} \tag{35}$$

4 WECC-CMLD PARAMETER DERIVATION

In power system load modelling, there are two main approaches to determine the parameters of the selected load model [5]: i) The component-based approach (see [6]) and ii) The measurement-based approach (see [7]). Both of these methods have advantages and disadvantages, therefore, in this deliverable, we take the advantages of both methods and use a hybrid approach to determine the parameters of the WECC-CMLD.

4.1 Component-based approach

The component-based load modelling aggregates the distribution of loads according to standard load classes and the load components of each class. In this approach, except for the load fractions, the parameters associated with each load component in the WECC-CMLD are fixed. Parameters are conventionally obtained based on past surveys or by averaging the values obtained from laboratory tests of common electrical appliances in residential, commercial and industrial facilities. The load fractions vary based on climate zones, seasons, time of the day and past surveys on the load composition in each of the created zone. The AEMO staff has made intensified efforts provide a rough estimation of the load composition (and the load fractions $F_{mA}, F_{mB}, F_{mC}, F_{mD}, F_{el}$) per state for winter and summer seasons. The derived load compositions are shown in Table 14 and Table 15. The remaining parameters, related to the transformer and distribution feeder (Section 3.2.1), induction motor A, B, C and D dynamics and protection (Section 3.2.2 and 3.2.3), power electronic loads (Section 3.2.4) and static loads (Section 3.2.5) are derived using previous studies on laboratory tests on different electrical devices for residential and commercial facilities.

Table 14: Load fractions obtained by AEMO (summer peak)

State	**Motor A** F_{mA}	**Motor B** F_{mB}	**Motor C** F_{mC}	**Motor D** F_{mD}	**Electronic Load** F_{el}
QLD	0.12	0.14	0.10	0.03	0.27
NSW	0.12	0.10	0.09	0.06	0.24
VIC	0.12	0.10	0.06	0.06	0.26
SA	0.09	0.13	0.11	0.05	0.35
TAS	0.14	0.12	0.13	0.03	0.15

4.2 Measurement-based approach

The component-based load model gives us a first estimation of the values of the parameters used in the WECC-CMLD. Nevertheless, due to the different types of electrical appliances

Table 15: Load fractions obtained by AEMO (winter peak)

State	Motor A F_{mA}	Motor B F_{mB}	Motor C F_{mC}	Motor D F_{mD}	Electronic Load F_{el}
QLD	0.06	0.12	0.11	0.03	0.19
NSW	0.04	0.08	0.08	0.06	0.20
VIC	0.04	0.08	0.07	0.06	0.20
SA	0.05	0.12	0.11	0.06	0.26
TAS	0.08	0.11	0.11	0.04	0.15

connected in distribution networks, changes in weather conditions and the distinct topological structure of distribution systems, these parameters are subjected to inaccuracies. If the parameters obtained using the component-based approach are given in vector $\mathbf{z}_0 \in \mathbb{R}^{N\times 1}$, we assume that each entry $z_i \in \mathbf{z}_0$ has an inherent error ϵ_i, and the actual parameter may fluctuate between $[z_i - \epsilon_i, z_i + \epsilon_i]$. With this in mind, the problem now is to estimate each $z_i \in [z_i - \epsilon, z_i + \epsilon]$ as to minimize the error between the active and reactive power of the WECC-CMLD and the active and reactive power obtained from measurements at each load bus.

We assume that the inputs (voltage and frequency at the load bus) and outputs (active and reactive power at the load bus) of the model in (32) and (33) are measured and represented by $\hat{\mathbf{v}}(t)$, $\hat{P}(t)$ and $\hat{Q}(t)$. The active and reactive power of the model at time t are given in equations (34) and (35). The model parameters $z_i \in \mathbf{z}$ can be estimated by minimizing the error between the model output and the measurements by solving the following non-linear optimization problem:

$$\min_{\mathbf{z}\in\mathbb{R}^{N\times 1}} \quad J(\mathbf{z}) = \int_{t_0}^{t_f} w_p \left(\hat{P}(t) - P_{cmld}(t, \mathbf{x}, \mathbf{z}, \mathbf{c}, \hat{\mathbf{v}}(t))\right)^2 dt + \int_{t_0}^{t_f} w_q(\hat{Q}(t) - Q_{cmld}(t, \mathbf{x}, \mathbf{z}, \mathbf{c}, \hat{\mathbf{v}}(t)))^2 dt \tag{36a}$$

$$\text{subject to} \quad \mathbf{z}_0 - \epsilon \leq \mathbf{z} \leq \mathbf{z}_0 + \epsilon, \tag{36b}$$

$$\mathbf{A}_{eq}\mathbf{z} = \mathbf{z_0} \tag{36c}$$

$$\mathbf{A}_{ineq}\mathbf{z} \leq \mathbf{b_{ineq}} \tag{36d}$$

The optimization problem consists of its objective function $J(\mathbf{z})$ in (36a), which represents the error between the output and the measurement data, a set of box constraints (36b), a set of equality constraints (36c) and a set of inequality constraints (36d). The variables w_p and w_q are user-defined weights assigned to active and reactive power. These weights represent the level of importance assigned to the active and reactive power outputs. The

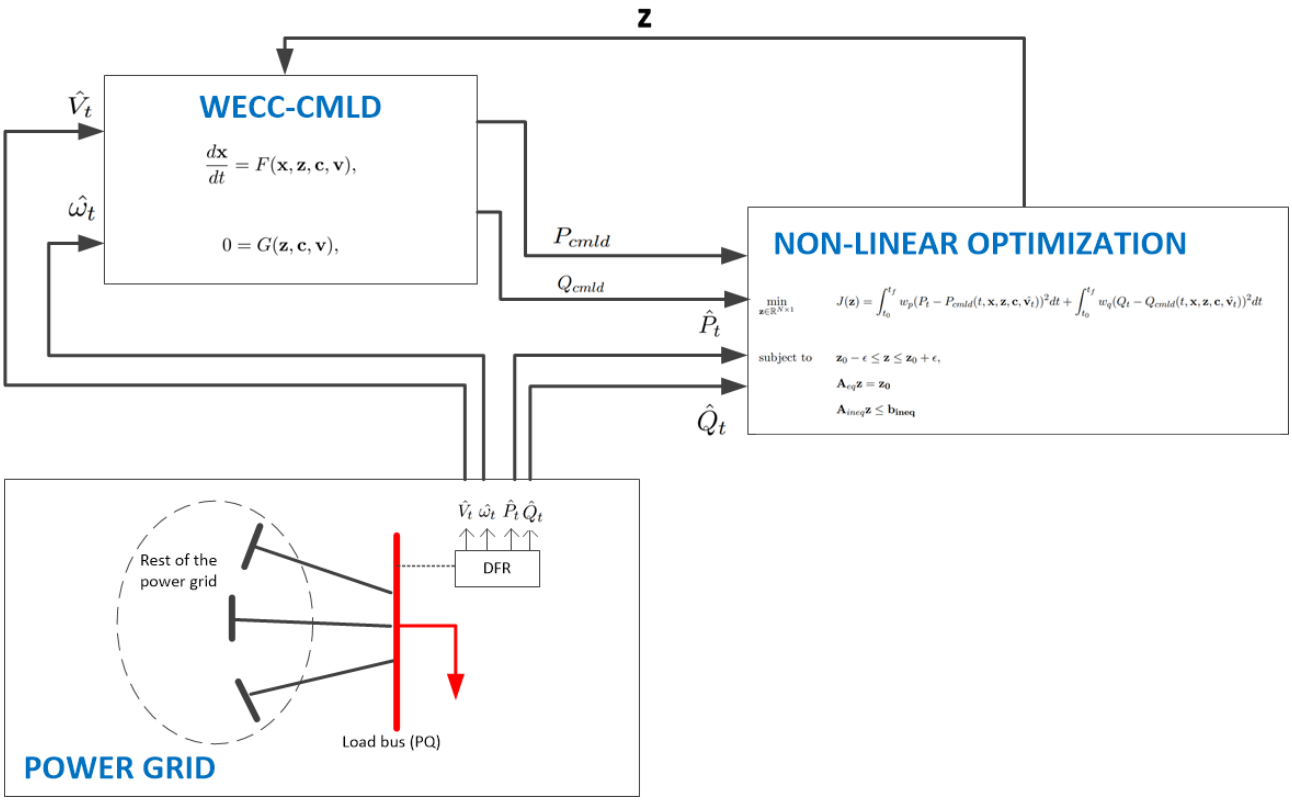

Figure 5: Developed measurement-based load model tool.

objective function consists of a system of non-linear differential and algebraic equations. The evaluation of the objective function requires a computationally expensive numerical integration method along with a Newton-Raphson algorithm to solve the network equations. Considering all parameters of the WECC-CMLD in the optimization problem (36a) is computationally unfeasible. Consequently, a hybrid a approach is followed in this deliverable. The approach consists of selecting a subset of parameters of the WECC-CMLD to be calibrated using measurement data. The remaining parameters are constants and their values are derived using the component-based approach (this can be done using the matrix $\mathbf{A}_{eq} \in \mathbb{R}^{N\times N}$ to add equality constraints on the fixed parameters in (36c)). One inequality constraint is added using matrix $\mathbf{A}_{ineq} \in \mathbb{R}^{1\times N}$ and vector $\mathbf{b}_{ineq} \in \mathbb{R}^{1\times 1}$ in equation (36d). This inequality constraint forces the summation of the load fraction parameters to be less than one ($F_{mA} + F_{mB} + F_{mC} + F_{mD} + F_{el} \leq 1$). The developed measurement-based load model is shown in Fig. 5.

4.3 Parameter Estimation Solution

4.3.1 Solution algorithm

The parameter estimation problem in equations (36a)-(36d) is solved using a Sequential Quadratic Programming (SQP) algorithm. SQP is one of the most powerful iterative algorithms for non-linear gradient-based optimization problems. An efficient implementation of the SQP algorithm in FORTRAN language [1] (also available in `scipy.optimize` by means of a `PYTHON` wrapper) is used in this deliverable.

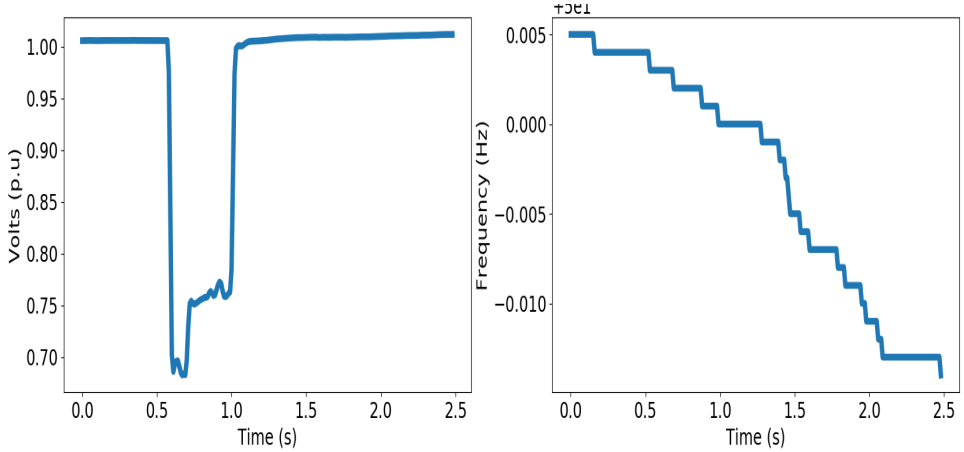

Figure 6: Brendale 14B event on October 21 2018 at 14:38.

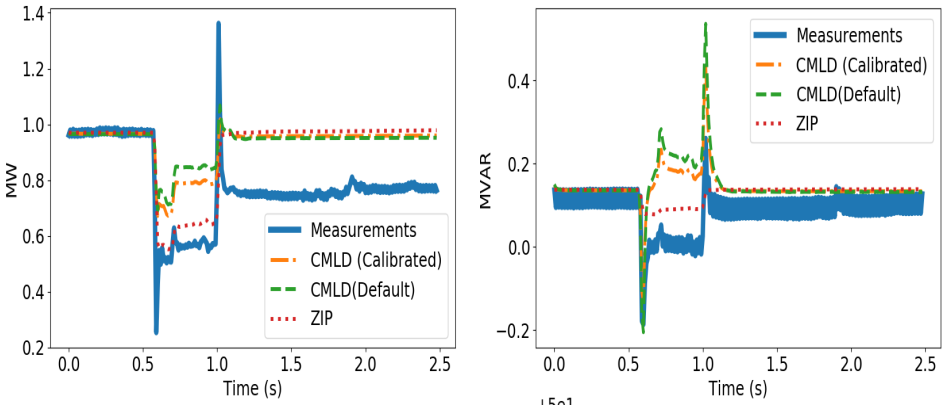

Figure 7: Estimation I: Active and reactive power outputs

4.3.2 Estimation I:

In this first experiment, we attempt to estimate 16 parameters—including the load fractions and the parameters of the static loads. All other parameters remain unchanged from their

component-based default values ($\mathbf{z}_0$) provided in Section 3. The parameters considered in the optimization problem (36a)-(36d) are: $F_{mA}, F_{mB}, F_{mC}, F_{mD}, F_{el}$, **PFs**, $P_{1e}, P_{1c}, P_{2e}, P_{2c}, P_{frq}, Q_{1e}, Q_{1c}, Q$ The selected disturbance occurred at Brendale 14B feeder on October 21, 2018 at 14:38:46. The voltage $\hat{V}_t$ and frequency $\hat{\omega}_t$ measurements captured by the DFR are depicted in Fig. 6. In this event, the objective function in (36a) using default parameters was found to be $J(\mathbf{z}_0) = 5.416$. The upper and lower bounds in (36b) for each parameter $z_i \in \mathbf{z}$ are $z_{0,i} + 0.25|z_{0,i}|$ and $z_{0,i} - 0.25|z_{0,i}|$ respectively—$z_{0,i} \in \mathbf{z}_0$ is the component-based default value of parameter i. As mentioned, one inequality constraint forces the summation of all load fractions to be less than one.

The SQP algorithm is used to minimize function $J(\mathbf{z})$ in an iterative manner. The algorithm converges in 7 iterations and the results of each iteration are given in Table 16 and Table 17. The value of $J(\mathbf{z})$ at every iteration is given in the last column of Table 17. As observed, $J(\mathbf{z})$ decreases from its initial value of 5.416 to the last value of 4.231. The WECC-CMLD outputs—with the default and calibrated parameters given in the first and last row of Tables 16 and 17 respectively—are depicted in Fig. 7. The results in Fig. 7 suggest that the selected parameters are unable to significantly reduce the error between the model outputs and the measurements. It is also observed that none of the models can emulate the observed reduction in active and reactive power after the fault is cleared.

Table 16: Estimation I: Parameters in each iteration

Iter	F_{mA}	F_{mB}	F_{mC}	F_{mD}	F_{el}
1	0.120	0.140	0.100	0.030	0.270
2	0.090	0.105	0.075	0.023	0.203
3	0.090	0.105	0.075	0.022	0.203
4	0.090	0.105	0.075	0.023	0.203
5	0.090	0.105	0.075	0.022	0.203
6	0.090	0.105	0.075	0.023	0.203
7	0.090	0.105	0.075	0.023	0.203

Table 17: Estimation I: Parameters in each iteration and objective function value

Iter	**PFs**	P_{1e}	P_{1c}	P_{2e}	P_{2c}	P_{frq}	Q_{1e}	Q_{1c}	Q_{2e}	Q_{2c}	Q_{freq}	$J(\mathbf{z})$
1	1.000	1.000	0.480	2.000	0.520	0.000	1.000	0.480	2.000	0.520	-1.000	5.416
2	0.990	1.250	0.600	2.347	0.650	0.000	1.043	0.573	2.041	0.650	-1.005	4.306
3	0.977	1.250	0.600	2.500	0.650	0.000	1.105	0.600	2.091	0.650	-1.007	4.268
4	0.960	1.250	0.600	2.500	0.650	0.000	1.206	0.600	2.170	0.650	-1.007	4.252
5	0.960	1.250	0.600	2.500	0.650	0.000	1.250	0.600	2.298	0.650	-1.000	4.242
6	0.960	1.250	0.600	2.500	0.650	0.000	1.250	0.600	2.500	0.650	-0.995	4.231
7	0.960	1.250	0.600	2.500	0.650	0.000	1.250	0.600	2.500	0.650	-0.995	4.231

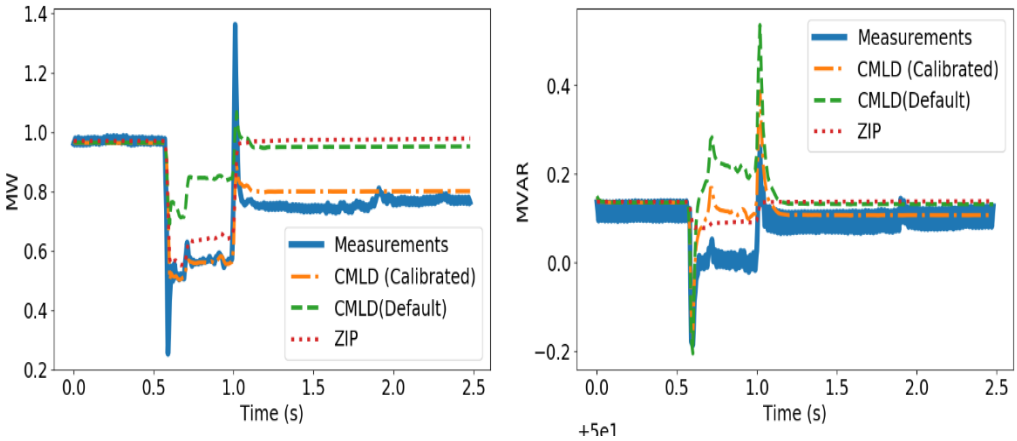

Figure 8: Estimation II: Active and reactive power outputs.

4.3.3 Estimation II

The reduction in active and reactive power observed in Fig. 7 is related to load tripping due to the action of the protection equipment of different appliances connected in the faulted feeder. Unfortunately, the default parameters assigned to the protection equipment of the different components in the WECC-CMLD cannot capture the load tripping behaviour for this disturbance. Therefore, the parameters of the protection equipment should be considered in the optimization problem (36a). In order to determine which protection parameters should be included in the error minimization problem, a sensitivity analysis was conducted. The sensitivity of the objective function $J(\mathbf{z})$ with respect to parameter z_i is calculated as $\frac{\partial J(\mathbf{z})}{\partial z_i}$. The most sensitive parameters were found to be: i) The first load tripping fraction of motor B (F_{tr1B}), ii)the first under-voltage tripping value of motor C (V_{tr1C}), iii) the first load tripping fraction of motor C (F_{tr1C}), iv) the fraction of power electronic loads that can recover (F_{rcel}), v) the voltage at which electronic loads start to drop (V_{d1}) and vi) the voltage at which all the electronic loads have dropped (V_{d2}). These protection parameters, together with the ones used in Estimation I, are calibrated in this experiment.

The optimization problem now has 22 variables in vector $\mathbf{z}$. The upper and lower bounds are identical to the ones indicated in Estimation I and the inequality constraint on the summation of the load fraction is maintained. The SQP algorithm converges in 18 iterations. The values of the calibrated parameters during the first and last five iterations are given in Table 18 and Table 19. The value of the objective function $J(\mathbf{z})$ is given in the last column of Table 19. It is observed that $J(\mathbf{z})$ decreases from its initial value of 5.416 to its final value of 0.829.

The active and reactive power outputs of the model with default and calibrated parameters are depicted in Fig. 8. As observed in this last figure, the WECC-CMLD clearly resembles the trajectory of the measurements for active and reactive power. This is because the protection parameters have been calibrated to emulate the under-voltage load tripping behaviour. Unfortunately, a small error is observed in the reactive power output at $0.6s < t < 0.9s$.

Table 18: Estimation II: Parameters and objective function

Iter.	F_{mA}	F_{mB}	F_{mC}	F_{mD}	F_{el}	V_{d1}	V_{d2}	P_{Fs}	P_{1e}	P_{1c}	P_{2e}
1	0.120	0.140	0.100	0.030	0.270	0.700	0.500	1.000	1.000	0.480	2.000
2	0.090	0.105	0.075	0.022	0.203	0.840	0.800	0.990	1.250	0.600	2.347
3	0.090	0.105	0.075	0.022	0.337	0.840	0.800	0.990	1.250	0.600	2.338
4	0.150	0.157	0.125	0.037	0.337	0.554	0.800	0.990	0.952	0.360	1.962
5	0.150	0.175	0.125	0.037	0.337	0.809	0.517	0.960	0.750	0.360	1.738
14	0.090	0.105	0.075	0.022	0.337	0.836	0.741	0.960	0.750	0.461	1.928
15	0.090	0.105	0.075	0.022	0.337	0.837	0.745	0.960	0.750	0.402	1.843
16	0.090	0.105	0.075	0.022	0.337	0.837	0.744	0.960	0.751	0.392	1.824
17	0.090	0.105	0.075	0.023	0.338	0.838	0.737	0.960	0.750	0.360	1.707
18	0.090	0.105	0.075	0.023	0.338	0.838	0.736	0.960	0.776	0.387	1.694

Table 19: Estimation II (cont.): Parameters and objective function.

Iter.	P_{2c}	P_{frq}	Q_{1e}	Q_{1c}	Q_{2e}	Q_{2c}	Q_{frq}	F_{tr1B}	V_{tr1c}	F_{tr2C}	F_{rcel}	$J(\mathbf{z})$
1	0.520	0.000	1.000	0.480	2.000	0.520	-1.000	0.000	0.580	0.000	0.800	5.416
2	0.650	0.000	1.043	0.573	2.041	0.650	-1.005	0.050	0.600	0.200	0.500	1.771
3	0.650	0.000	1.071	0.600	2.062	0.650	-1.007	0.050	0.600	0.200	0.500	1.101
4	0.390	0.000	1.181	0.600	2.142	0.650	-1.010	0.050	0.600	0.200	0.500	7.735
5	0.390	0.000	1.160	0.600	2.123	0.650	-1.006	0.050	0.600	0.200	0.500	3.190
14	0.390	0.000	1.250	0.600	2.500	0.650	-1.006	0.050	0.600	0.200	0.500	0.831
15	0.390	0.000	1.250	0.600	2.500	0.650	-1.008	0.050	0.600	0.200	0.500	0.830
16	0.390	0.000	1.250	0.600	2.500	0.650	-1.008	0.050	0.600	0.200	0.500	0.829
17	0.390	0.000	1.250	0.600	2.500	0.650	-1.007	0.050	0.600	0.200	0.500	0.829
18	0.390	0.000	1.250	0.600	2.500	0.650	-1.005	0.050	0.600	0.200	0.500	0.829

Table 20: Estimation III: Solution when extending the upper and lower bounds of the parameters

Parameter	Lower Bound	Upper Bound	Default	Calibrated
F_{mA}	0	0.3	0.12	0.231
F_{mB}	0	0.3	0.14	0.000
F_{mC}	0	0.3	0.1	0.000
F_{mD}	0	0.1	0.03	0.000
F_{el}	0.203	0.7	0.27	0.403
V_{d1}	0.3	0.84	0.7	0.840
V_{d2}	0.2	0.8	0.5	0.739
P_{Fs}	0.96	0.99	1	0.960
P_{1c}	0.15	0.6	0.48	0.150
P_{2c}	0.15	0.8	0.52	0.150
P_{frq}	0	2	0	1.047
Q_{1c}	0.1	1.8	0.48	1.800
Q_{2c}	0.3	1.5	0.52	1.500
Q_{frq}	-1.2	-0.8	-1	-1.005
F_{tr1}	0.05	0.6	0	0.550
V_{tr1}	0.5	0.8	0.58	0.620
F_{tr2}	0.2	0.9	0	0.759
F_{rcel}	0.5	0.96	0.8	0.500
J(z)	0	Inf	5.416	0.483

4.3.4 Estimation III

In the previous two estimations, we calibrated all static load parameters in the optimization process. The physical interpretation of static loads, however, is to represent loads with with constant impedance and constant current. Constant current loads are represented by $P_{1e} = Q_{1e} = 1$ and constant impedance loads are emulated using $P_{2e} = Q_{2e} = 2$. Although the user can modify these four parameters, in order to preserve their physical meaning, we will keep them as constants in this numerical experiment. In addition, aiming to further reduce the value of the objective function, we will extend the upper and lower bounds of the remaining parameters in the calibration process. The selected bounds of each parameter are given in second and third columns of Table 20. The default and calibrated values of each parameter after convergence of the SQP algorithm are given in the fifth and sixth columns of the same table respectively. The last row of Table 20 indicates that, by allowing the parameters to change in a wider range, function $J(\mathbf{z})$ can be minimized to 0.483 . A comparison between the output of the model and the measurements is given in Fig. 9, where both the active and reactive power now resemble the trajectory of the measurements more accurately than the previous two estimations.

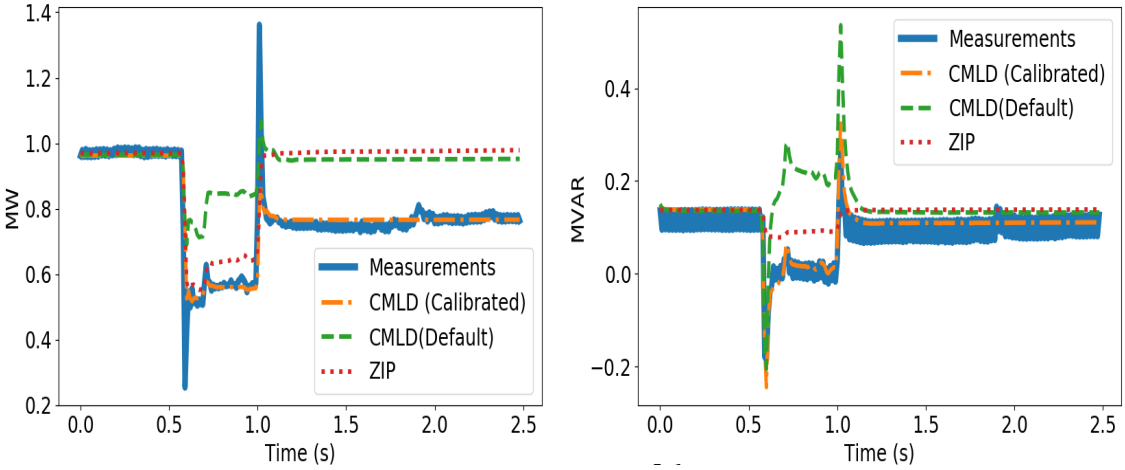

Figure 9: Estimation III: Active and reactive power outputs.

Table 21: Obtained parameters for additional experiments on various events.

Parameter	Event 1	Event 2	Event 3	Event 4
F_{mA}	0.109	0.000	0.000	0.001
F_{mB}	0.222	0.160	0.179	0.115
F_{mC}	0.000	0.000	0.000	0.000
F_{mD}	0.000	0.001	0.000	0.000
F_{el}	0.329	0.301	0.596	0.203
V_{d1}	0.840	0.840	0.787	0.355
V_{d2}	0.453	0.332	0.375	0.258
P_{Fs}	0.960	0.960	0.960	0.960
P_{1c}	0.515	0.580	0.150	0.600
P_{2c}	0.392	0.738	0.150	0.800
P_{frq}	1.692	1.049	0.901	0.727
Q_{1c}	1.800	1.784	1.784	1.265
Q_{2c}	1.500	1.500	1.071	1.497
Q_{frq}	-0.904	-0.805	-1.040	-0.862
F_{tr1}	0.208	0.417	0.050	0.076
V_{tr1}	0.657	0.716	0.733	0.695
F_{tr2}	0.364	0.343	0.272	0.584
F_{rcel}	0.834	0.621	0.866	0.719
J($\mathbf{z}_0$)	7.199	8.78	33.85	1.007
J($\mathbf{z}^*$)	1.622	0.980	2.660	0.258

4.3.5 Additional Experiments

In this section, we estimate the WECC-CMLD parameters using data of different disturbances in Australia. An identical approach to the one explained in Section 4.3.4 was conducted, where the lower and upper bounds as well as the default values of the parameters are given in Table 20. The solutions obtained by the SQP algorithm are summarized in Table 21. The four selected events are described as follows:

1. The first event occurred at Brendale 11A feeder on January 4, 2018 at 20:27:39. The output of the model with calibrated and default parameters is shown in Fig. 10. The obtained parameters are given in the second column of Table 21. After convergence, the objective function was reduced from 7.199 to 1.622.

2. The second event took place at Brendale 11A feeder on May 1, 2018 at 17:25:30. The output of the model with calibrated and default parameters is shown in Fig. 11. The obtained parameters are given in the third column of Table 21. After convergence, the objective function was reduced from 8.780 to 0.980.

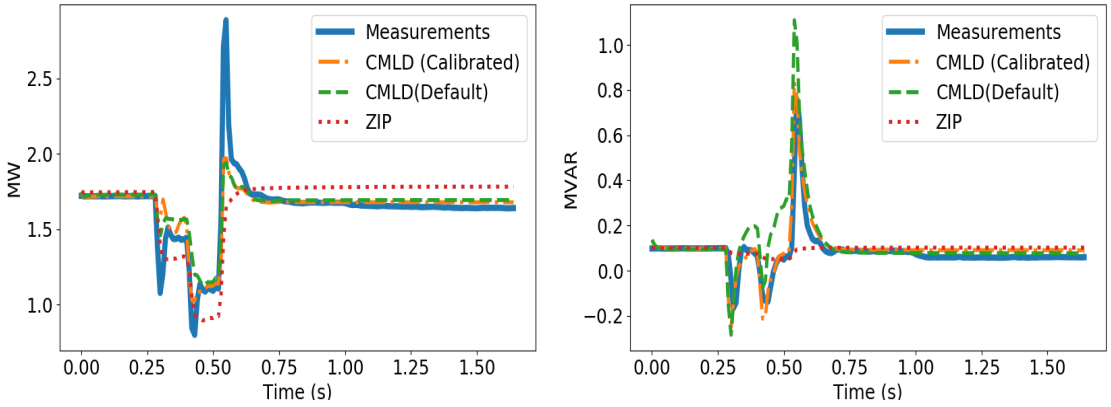

Figure 10: Event 1: Brendale 11A January 4 2018 at 20:27:39

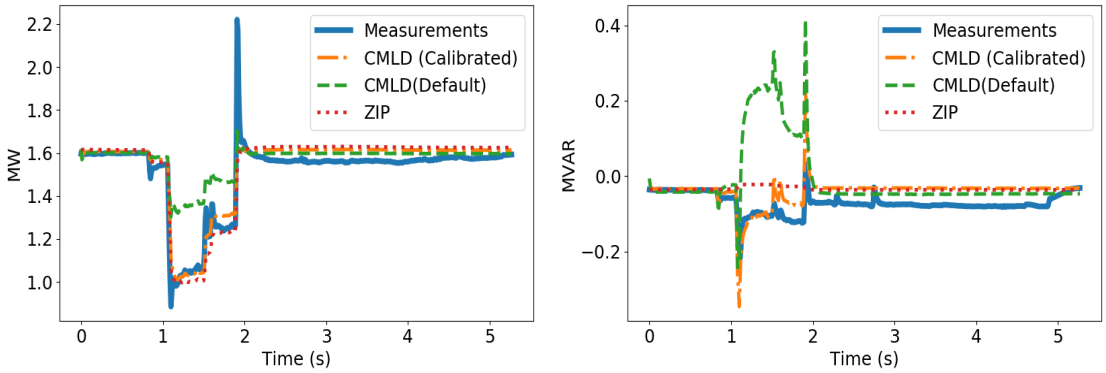

Figure 11: Event 2: Brendale 11A May 1, 2018 at 18:27:38

3. The third event took place at Brendale 11A feeder on June 19, 2018 at 17:26:09. The output of the model with calibrated and default parameters is shown in Fig. 12. The values of the calibrated parameters are shown in the fourth column of Table 21. After convergence, the objective function was reduced from 33.850 to 2.660.

4. The fourth event took place at Brendale 11A feeder on Brendale 11A July 31, 2018 at 22:51:24. The output of the model with default and calibrated parameters is shown in Fig. 13. The calibrated parameters are given in the last column of Table 21. The objective function was reduced from 1.007 to 0.258.

As observed in Figs. 10, 11, 12 and 13, the calibrated WECC-CMLD outperforms the model with default parameters and the conventional ZIP model.

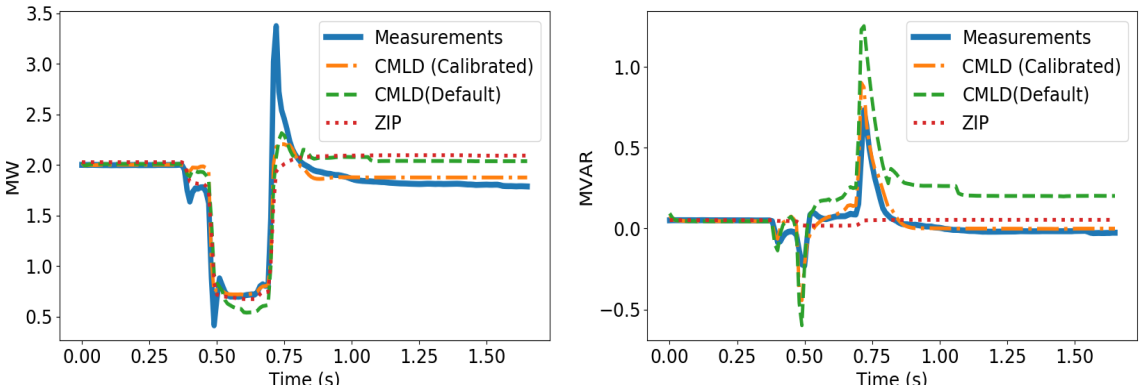

Figure 12: Event 3: Brendale 11A June 19 2017 at 17:25:38

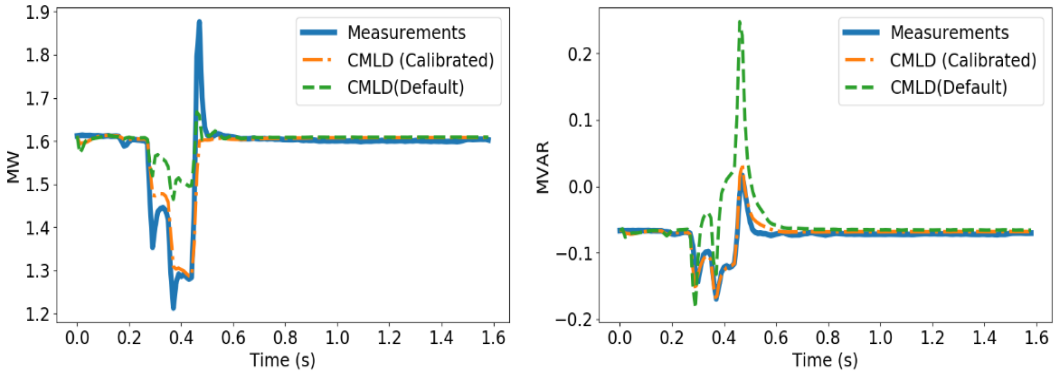

Figure 13: Event 4: Brendale 11A July 31, 2018 at 22:51:24

4.4 Future Work

4.4.1 WECC-CMLD Parameter Estimation

Our results indicate the the hybrid component-based and measurement-based approach for estimating the parameters of the WECC-CMLD leads to a better emulation of aggregate behaviour of loads at different feeders in Australia. The component-based approach alone seems unable to accurately capture the dynamics of the load for different types of disturbances, it requires a measurement-based approach to calibrate its parameters according to the particular type of disturbance, time of the day, weather conditions and so on. The measurement-based approach, however, needs further improvements. Thus far, the WECC-CMLD parameters are calibrated separately for each disturbance. In the next few months, the measurement-based approach will be modified as to consider multiple disturbances simultaneously to calibrate the parameters of the WECC-CMLD. More specifically, if measurements from more than one disturbance are considered and the data of disturbance k are represented as $\hat{\mathbf{v}}_k(t)$, $\hat{P}_k(t)$ and $\hat{Q}_k(t)$, the objective function of the measurement-based approach will be modified as follows:

$$J(\mathbf{z}) = \sum_{k=0}^{K} \left(\int_{t_{k,0}}^{t_{k,f}} w_{k,p}(\hat{P}_k(t) - P_{cmld}(t, \mathbf{x}, \mathbf{z}, \mathbf{c}, \hat{\mathbf{v}}_k(t)))^2 dt + \int_{t_{k,0}}^{t_{k,f}} w_{k,q}(\hat{Q}_k(t) - Q_{cmld}(t, \mathbf{x}, \mathbf{z}, \mathbf{c}, \hat{\mathbf{v}}_k(t)))^2 dt \right). \tag{37}$$

The above problem requires further developments in the computational tool. It is also k times more computationally expensive than the current measurement-based approach.

4.4.2 Incorporation of DER Dynamics

The aggregate dynamics of DER represented by the DER_A model (presented in the Milestone1 report) will be added in the parameter calibration process. The new output considering the dynamics of DER_A will be derived and incorporated in the total active and reactive power output of the model in equations (34) and (35). In the next release of the parameter calibration tool, the parameters of DER_A will be included in the optimization algorithm.

5 LOAD MODELLING UPDATE

This section focusses on the progress since the last milestone, which consisted in incorporating the distributed energy resource DER_A component into the composite PV-load model. The information and results presented in Section 4 regarded only the load component of the composite PV-load model, without addressing the DER component.

The tool which estimates the parameters of the composite PV-load model has been updated to include the DER_A parameters and some results are presented in this section. This tool estimates the parameters of the WECC composite load model based on a *hybrid optimization* approach, making use of conventional nonlinear programming solvers and a recently developed derivative free optimization technique from [16]. In addition, unlike previous works, physical constraints on the parameters are imposed in order to limit the number of feasible solutions.

The parameter estimation problem is based on the formulation expressed in (37), where an objective function based on the (quadratic) difference between measured and computed active and reactive power is minimized. The computed powers are the output of the composite PV-load model, with parameters tuned by the developed tool.

The plots in Fig. 14 display the results from a grid event where no load tripping was recorded, whereas the plots in Fig. 15 represent the model results when a load tripping event was observed. In either case the optimized model outputs a result that mimics closely the measured values of active and reactive power and performs significantly better than the model with default parameters.

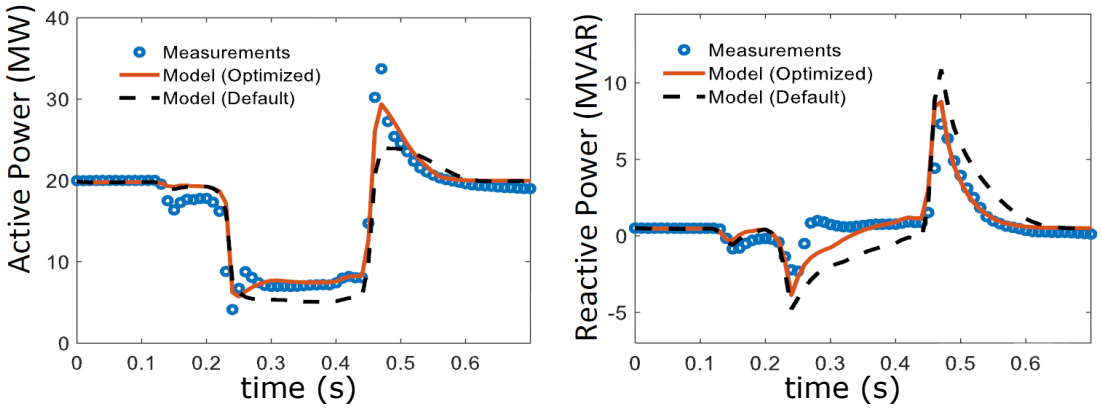

Figure 14: Composite PV-load model result, grid event without load tripping

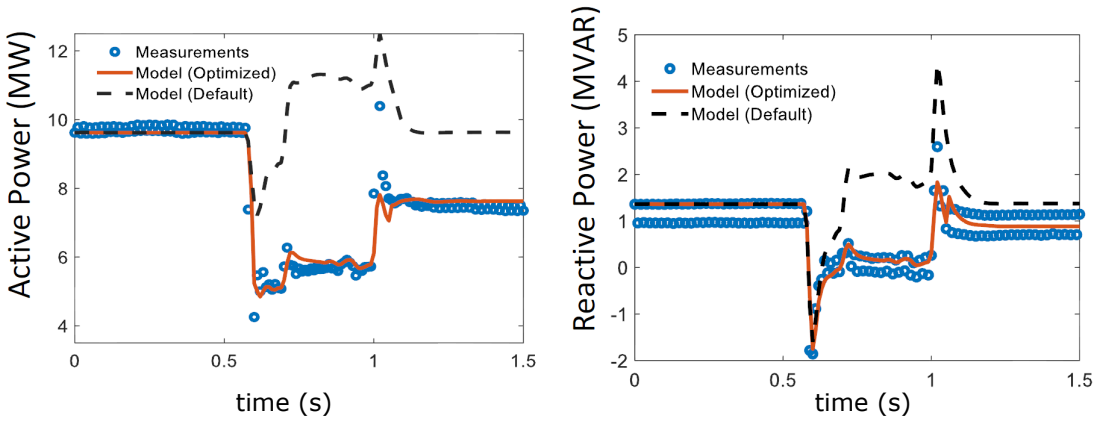

Figure 15: Composite PV-load model result, grid event with load tripping

6 CONCLUSIONS AND PROJECT PRIORITIES

6.1 Conclusions

During the past six months (milestone 3 reporting period) we have continued the bench-testing process of PV inverters, and confirmed that certain types of grid disturbances are detrimental to the correct operation of inverters, causing disconnection or power curtailment. On the load modelling end, the effort was spent to embed the aggregate inverter component (DER_A model) into the composite load model (CMLD) and calibrating parameters of the whole model.

Based on inverter bench testing results and the DER-load modelling work, we can highlight the following facts:

- We continued to observe a wide variety of inverter behaviours. This presents a challenge to the development of a single aggregate model for all PV inverters. The load model parameters must be tuned considering that a percentage of inverters, and not all, display unusual behaviours in response to grid disturbances.
- Sub-cycle threats such as grid voltage phase-angle jumps and short-duration voltage sags remain challenging to represent in the composite PV-load model, considering that this is implemented in software (PSS/E) that works on steady-state phasor-analysis of positive sequence voltage components only.
- Our understanding of inverter behaviours based on grid incidents using combinations of high-frequency data, Solar Analytics data, and bench testing is improving. However, we need to increase our knowledge of the distribution grid and especially how disturbances are transferred from the transmission to the distribution layers of the power systems, where rooftop inverters are connected. The role of transmission/distribution lines and transformer connections may also have an impact on the disturbances propagation.
- The electrical parameters of induction motors A, B and C in the WECC-CMLD may help us to provide a better fit between the model output and the measured data. An attempt to calibrate these parameters should be conducted. This however requires the integration of additional constraints and bounds in the optimization problem.

6.2 Project priorities for next six months (reporting period up to Milestone 4)

The project priorities for the next six months have been established upon discussions with the steering committee (AEMO, ElectraNet and TasNetworks) and industry advisory group, and are a result of emerging needs in understanding inverter behaviours based on bench testing results and progress needed in the load modelling, considering also that AEMO has invested internal resources to advance the development of the PV-composite load model.

1. Conduct further under-voltage testing in the fleet of single-phase PV inverters tested thus far, regarding response to short-duration voltage sags. The current results on short-duration voltage sag, tested the inverter response when subjected to a 230 to 50 V sag (about 0.8p.u.) for 100 ms. The new tests will have a finer resolution, performing sags of magnitude from 0.9 p.u. to 0.2 p.u., in steps of 0.1 p.u., and durations of 80 ms, 120 ms and 220 ms, conforming to the fault clearing times reported in the National electricity Rules, chapter 5, Table S5.1a.2 [17, p. 546].
2. Verify the entire start-up behaviour of inverters tested thus far. In the tests carried out so far the start-up power ramp of the inverters has not been verified for the full six minutes duration due to limitations in the size of the data files collected. In the next batch of tests the entire start-up procedure (1min delay plus 16% power increase per minute is to be recorded).
3. Test inverter behaviour when connected to a weak grid. This aspect was discussed with the steering committe, however further investigation is needed to translate a weak grid condition into the inverter becnh testing setup.
4. Test the Volt-Var power quality mode of inverters. As this mode is not enabled by default, members of the industry advisory group have asked to test it, to observe the behavior of the inverter when this is delivering 1 p.u. of active power and the ac voltage is such that the Volt-Var response must be enabled.
5. Contribute to the activity of EL-42 of Standards Australia in updating AS 4777.2.

Whilst the above items are of high-priority, the list below is providing other topics of interest to help the success of the project:

- Testing of new PV inverters, including hybrid PV/battery inverters and three-phase inverters. Process data and report writing for each inverter.

- Hardware in the loop testing: develop network model in RTDS and interface it to inverter testing setup, simulating typical fault scenarios and propagation of faults from transmission to distribution grid.
- More profound testing on PV inverters to be conducted in order to derive the inverter's frequency estimation mechanism (PLL or zero-crossing techniques) and possibly other grid-support function such as Volt-Var and Watt-frequency responses.
- Develop an automated disturbance monitoring program. The program should automatically detect the minimum voltage drop per phase, the active/ reactive power before and after the disturbance and the unbalance ratio.
- Support of measurements from multiple disturbances in the parameter calibration algorithm.
- Calibration of additional parameters in the WECC-CMLD model to obtain a closest match between the PMU measurements and the model output.
- Parameter estimation of DER_A and WECC composite load model simultaneously. Requires additional software developments.
- Integration of the DER_A model into the load model parameter estimation algorithm requires further work.
- Modifications to the DER_A model to support different versions of the AS4777 standard. This requires the development of the entire DER_A model in Fortran language to be supported by Siemens/PTI.
- Add the RoCoF effects into the DER_A model. This requires the addition of a new partial RoFoC tripping block into the new DER_A model in Fortran language.
- Comparisons between PMU devices and Wattwatchers ($6k$ + vs cost of WW device)

References

[1] D. Kraft, *A Software Package for Sequential Quadratic Programming* Forschungsbericht. Deutsche Forschungs- und Versuchsanstalt für Luft- und Raumfahrt, DFVLR, 1988

[2] Qiuhua Huang and Renke Huang and Bruce J. Palmer and Yuan Liu and Shuangshuang Jin and Ruisheng Diao and Yousu Chen and Yu Zhang *A Reference Implementation of WECC Composite Load Model in Matlab and GridPACK*, http://arxiv.org/abs/1708.00939

[3] *Grid Connection of Energy Systems via Inverters. Part 3: Grid Protection Requirements*, Standards Australia/Standards New Zealand Std. AS 4777.3, 2005.

[4] *Grid Connection of Energy Systems via Inverters. Part 2: Inverter Requirements*, Standards Australia/Standards New Zealand Std. AS 4777.2, 2015.

[5] Z. Y. Dong, A. Borghetti, K. Yamashita, A. Gaikwad, P. Pourbeik, J. V. Milanović *CIGRE WG C4.065 Recommendations on Measurement Based and Component Based Load Modelling Practice* in Fusion of Lightning Research and Practice for Power System in the Future; 10 Oct 2012-12 Oct 2012; Hakodate, Japan. 2012.

[6] Anish Gaikwad, Penn Markham, Pouyan Pourbeik *Implementation of the WECC Composite Load Model for utilities using the component-based modeling approach* in IEEE TIEEE/PES Transmission and Distribution Conference and Exposition (T&D), May 2016

[7] Jae-Kyeong Kim, Kyungsung An, Jin Ma, Jeonghoon Shin, Kyung-Bin Song, Jung-Do Park, Jung-Wook Park, Kyeon Hur *Fast and Reliable Estimation of Composite Load Model Parameters Using Analytical Similarity of Parameter Sensitivity* in IEEE Transactions on Power Systems, vol. 31, NO. 1, January 2016.

[8] AEMO *Technical Integration of Distributed Energy Resources: Improving DER capabilities to benefit consumers and the power system*, https://www.aemo.com.au/-/media/Files/Electricity/NEM/DER/2019/Technical-Integration/Technical-Integration-of-DER-Report.pdf, April 2019.

[9] Western Electricity Coordinating Council *WECC Dynamic Composite Load Model (CMPLDW) Specifications* https://www.wecc.biz/Reliability/WECC

[10] Q. Huang, R. Huang, B.J. Palmer, Y. Liu, S. Jin, R. Diao *A generic modelling and development approach for WECC composite load model* Electric Power System Research 172(2019) 1-10

[11] Georgios Konstantinou, Leonardo Callegaro, John Fletcher, Nelson Avila *From inverter standard to inverter behaviour for small-scale distribted generation* Asia Pacific Conference for Integration of Distributed Energy Resources (CIDER), Melbourne, 20-21 Aug. 2019.

[12] www.cleanenergyregulator.gov.au, accessed July 2019.

[13] pv-map.apvi.org.au/postcode, accessed July 2019.

[14] N. Stringer, N. Haghdadi, A. Bruce, J. Riesz and I. MacGill, *Observed behavior of distributed photovoltaic systems during major voltage disturbances and implications for power system security*, Applied Energy, Volume 260, 2020

[15] Quint, R., et al., Transformation of the Grid: The Impact of Distributed Energy Resources on Bulk Power Systems, *IEEE Power and Energy Magazine* 17(6), 2019, pp. 35-45

[16] A. Costa, E. Di Buccio, M. Melucci, and G. Nannicini, "Efficient parameter estimation for information retrieval using black-box optimization," *IEEE Transactions on Knowledge and Data Engineering*, vol. 30, no. 7, p. 12401253, Jul 2018

[17] National Electricity Rules, Version 103, Chapter 5, Network Connection and Planning Expansion, https://www.aemc.gov.au/sites/default/files/content//NER-v103-Chapter-05.PDF, accessed Feb. 2020

Contact: John Fletcher

Email: john.fletcher@unsw.edu.au

END